

UNIVERSITY OF CALGARY

FRACTURING IN UNCONSOLIDATED BITUMEN RESERVOIRS
DURING STEAM INJECTION

by

Derry B. Eddy

A THESIS SUBMITTED TO
THE FACULTY OF GRADUATE STUDIES
IN PARTIAL FULFILMENT OF THE REQUIREMENTS FOR THE
DEGREE OF MASTERS OF SCIENCE

DEPARTMENT OF CHEMICAL AND PETROLEUM ENGINEERING
CALGARY, ALBERTA, MAY 1992

© Derry Eddy 1992



National Library
of Canada

Acquisitions and
Bibliographic Services Branch

395 Wellington Street
Ottawa, Ontario
K1A 0N4

Bibliothèque nationale
du Canada

Direction des acquisitions et
des services bibliographiques

395, rue Wellington
Ottawa (Ontario)
K1A 0N4

Your file *Votre référence*

Our file *Notre référence*

The author has granted an irrevocable non-exclusive licence allowing the National Library of Canada to reproduce, loan, distribute or sell copies of his/her thesis by any means and in any form or format, making this thesis available to interested persons.

L'auteur a accordé une licence irrévocable et non exclusive permettant à la Bibliothèque nationale du Canada de reproduire, prêter, distribuer ou vendre des copies de sa thèse de quelque manière et sous quelque forme que ce soit pour mettre des exemplaires de cette thèse à la disposition des personnes intéressées.

The author retains ownership of the copyright in his/her thesis. Neither the thesis nor substantial extracts from it may be printed or otherwise reproduced without his/her permission.

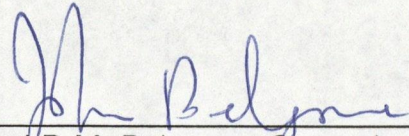
L'auteur conserve la propriété du droit d'auteur qui protège sa thèse. Ni la thèse ni des extraits substantiels de celle-ci ne doivent être imprimés ou autrement reproduits sans son autorisation.

ISBN 0-315-79131-4

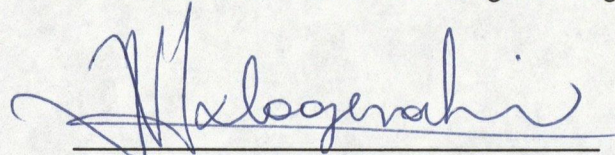
Canada 

THE UNIVERSITY OF CALGARY
FACULTY OF GRADUATE STUDIES

The undersigned certify that they have read, and recommended to the Faculty of Graduate Studies for acceptance, a thesis entitled, "Fracturing in Unconsolidated Bitumen Reservoirs During Steam Injection", submitted by Derry B. Eddy in partial fulfilment of the requirements for the degree of Master of Science.



Dr. J.D.M. Belgrave, Supervisor
Chemical and Petroleum Engineering



Dr. N.E. Kalogerakis
Chemical and Petroleum Engineering



Dr. R.G. Moore
Chemical and Petroleum Engineering



Dr. I. Wierzba
Mechanical Engineering

May 8, 1992

Abstract

The very viscous nature of bitumens dictates the need for the injection of steam into the reservoir to mobilize the bitumen. The permeability of the reservoir matrix to steam is usually very poor and the result is the formation of fractures. The simulation of these fractures is the focus of this work.

The new fracture model developed in this work provides a mechanism which accounts for a number of important phenomena observed during the cyclic steam process. These are:

- a) Surface heave with vertical fractures.
- b) The high energy required to propagate the fracture tip into these sands, which have low tensile strength.
- c) Gravity override of the fractures.
- d) Greater dispersion of the energy with increased injection rates.
- e) Hysteresis between the injected and produced water.

Implementation of the model allows the study of the injection of a hydrocarbon gas along with the steam. Also, the method employed provides a means to estimate the dispersion in the reservoir from the production data. Furthermore, as a consequence of the dispersive nature of the fracture flow, larger time steps can be used by the simulator.

Acknowledgements

I would like to thank many people whose help made the completion of this work possible. In particular, I would like to thank:

My thesis supervisor, Dr. John Belgrave, for his encouragement, assistance and support throughout this work.

Fellow graduate students, who have made this experience especially rewarding. Special thanks must be extended to P.G. Sriram for sharing some of his knowledge and experience with me.

All of the secretarial staff in the Department of Chemical and Petroleum Engineering.

Last, but not least, my wife, Sheila, for her support and encouragement.

Table of Contents

Approval Page	ii
Abstract	iii
Acknowledgement	iv
Table of Contents	v
List of Table	viii
List of Figures	ix
Nomenclature	x

Chapter 1 - Introduction **1**

1.1 Reservoir Simulation	1
1.2 Reservoir Models	2
1.3 Computer Time Requirements	3
1.4 Gradients, Nonlinearities and Grid Block Size	3
1.5 Fracturing	5
1.6 Objective of Study	6

Chapter 2 - Literature Review and Development of Fracturing Concept **8**

2.1 Thermal Reservoir Models, Darcy Flow Only	8
2.2 Correlations	13
2.3 Pseudo Functions	15
2.4 General Reference	16
2.5 Hydraulic Fracturing in Consolidated Sands	16
2.6 The Nature of Fracturing in Oil Sands	20
2.6.1 Matrix Disruption	22
2.6.2 Hydraulic Fracturing of Unconsolidated Sands	24
2.6.3 Other Thermal Fracturing Models	24
2.6.4 Ito's Dispersion Model	25
2.6.5 Review of In-Situ Pilots in Athabasca Tar Sands and Implication of Data	29
2.7 Fracturing Concept	32

Chapter 3 - The Simulator	36
3.1 Overview	36
3.2 Numerical	38
3.2.1 Equation Set	38
3.2.2 Matrix Solution	40
3.3 Formulation	44
3.3.1 Absence of Oxygen or Other Non-condensable Gas Component	46
3.3.2 Asphaltenes and Maltenes Component Balance Dependencies	46
3.3.3 Absence of the Gas Component	48
3.3.4 Liquid Water Disappears	49
3.3.5 Thermodynamic Consistency	49
3.4 Fracturing Numerical Model Development	51
3.4.1 Relevant Information on Fractures in Unconsolidated Sands	51
3.4.1.1 Liquid Water Flow	51
3.4.1.2 Direction of Fracture Flow and Gravity Override	54
3.4.2 Numerical Models Investigated	57
3.4.2.1 Fracturing Model Overview	58
3.4.3 Numerical Model Development Constraints	60
3.4.4 Numerical Model Concept	61
3.4.5 Assumptions	63
1. The Fracture Makes Its Own Permeability	63
2. Only Gas Flows in Fractures	64
3. Volume of the Fractures is Zero	67
4. Fracture Temperature is Saturated Steam Temperature	68
5. Heat Transferred to Matrix is Heat Conduction Limited	68
6. Fracture Pressure Gradient can be Estimated from Rock Opening Pressure	69

3.4.6 Implementation	73
3.4.6.1 Mass and Heat Exchange Between Matrix and Fracture	76
3.4.6.2 Division of Enthalpy and Mass Flow in Downstream Fractures	77
3.4.6.3 Simulator's Matrix Disruption	78
3.4.7 Model Evaluation	78
3.4.8 History Matching Fracture Parameters	79
3.4.9 The Second and Subsequent Cycles	81
Chapter 4 - Simulation	82
Chapter 5 - Results and Discussion	91
5.1 Sensitivity Studies for Fracture Parameters	91
5.1.1 Dispersion Coefficient	91
5.1.2 The Pressure Gradient Temperature Correction	95
5.2 Fracture Growth	96
5.3 The Effect of Injection Rate on the Temperature Distribution	99
5.4 The Effect of a Gas Phase on the Production	99
5.5 The Effect of Grid Size on the Production Curves	103
5.6 The Effect of Injection of Ethane on the Oil Viscosity	105
5.7 History Match to Cold Lake Data	107
Chapter 6 Conclusions and Recommendations	112
References	114
Appendix A - Conservation Equation for the Matrix	119
Appendix B - Maltenes Siding Scale	122
Appendix C - Condensible Gas Sliding Scale	124
Appendix D - Computer Time	126
Appendix E - Water Correlation	127

List of Tables

2.1 Alignment of Conservation Equations with Primary Variables	11
4.1 Relative Permeability Curves, Test Case	88
4.2 History Match Parameters for Cold Lake Production	89
4.3 Relative Permeability Curves, Cold Lake Reservoir	90
5.1 Effects of Dispersion on Production of Bitumen	93
5.2 Temperature Correction $v_T = 0.0001$, Case 1	93
5.3 Temperature Correction $v_T = 0.002$, Case 2	95
5.4 Fracture Temperature	98
5.5 Case 1, Viscosity (Pa s) with Dissolved Ethane Considered	106
5.6 Case 2, Viscosity (Pa s) without Solution Gas Viscosity	106

List of Figures

Figure 1	Rock Stress on a Vertical Fracture	17
Figure 2	Surface Heave and Pore Pressure	21
Figure 3	Ito's Fracturing Concept	27
Figure 4	Fracturing Concept	33
Figure 5	Natural Grid Ordering	41
Figure 6	D4 Ordering	43
Figure 7	Mollier Diagram of Water	52
Figure 8	Vertical Fracture Through Two Grid Blocks	55
Figure 9	Numerical Model Concept	62
Figure 10	Effects of Dispersion Coefficient on the Temperature of the Produced Fluids	92
Figure 11	Fracture Growth	97
Figure 12	Effect of Injection Rate on Reservoir Matrix Temperature	100
Figure 13	Gas Saturated Production	101
Figure 14	Unsaturated Reservoir Production	102
Figure 15	Unsaturated Reservoir Production (Two grid Blocks in Vertical Direction)	104
Figure 16	First Cycle History Match, Oil Production Rate	109
Figure 17	First Cycle History Match, Cumulative Oil and Water Production	110

Nomenclature

A	Area (m^2)
A_d	Area per gradient length per volume (m^{-2}), associated with injection block.
A_0, A_1	Viscosity interaction Parameters
b_1, b_2	Viscosity parameters
B	Binary viscosity interaction parameter
CN	Carbon number of gas
CNI	Initial carbon number of gas dissolved in the bitumen
E	Young's modulus (Pa)
$efac$	Exponential factor
$f, A1, B1$	Functions
F	Fraction
g	Gravitational constant ($9.81 m/s^2$)
H	Enthalpy (kJ/kmole)
H_{sl}	Enthalpy saturated liquid water (kJ/kmole)
H_{sv}	Enthalpy saturated water vapour (kJ/kmole)
z	Height (m)
I	Amperage, Flow rate (kmoles/s)
K_{ij}	Phase distribution coefficient i in j phase
K_f	Fracture permeability (m^2)
K	Matrix permeability (m^2)

k_r	Relative permeability
k_c	Thermal conductivity
k_{rg}	Relative permeability of gas
k_{rog}	Relative permeability of oil to gas
k_{row}	Relative permeability of oil to water
k_{rw}	Relative permeability of water
M_f	Heat capacity (kJ/(m ³ °C))
M_{kw}	Molecular weight of k
N_c	Number of components
N_{eq}	Number of equations per grid block
N_p	Number of Phases
N_x	Number of grids in x direction
N_y	Number of grids in y directions
N_{rea}	Number of reactions
P	Pressure (Pa)
q_i	Mass injection or production rate of i (kmoles/s)
Q	Rate of heat transferred between matrix and fraction or heat produced or injected (J/s)
R	Resistance
sl	1.0 minus the Gas Saturation
S_w	Saturation of water
S_o	Saturation of oil

S_g	Saturation of gas
T	Temperature ($^{\circ}\text{C}$ or K)
t	Time (s)
U	Internal Energy (kJ/kmole)
V	Volume of grid block (m^3)
X	Steam quality
X_i	Master phase mole fraction of i
x_{ij}	Mole fraction of component i in the j phase
x	Length (m)
$xfac$	Fraction of gas in oil, compared to initial case.
y	Mole fraction
z	Distance in the vertical direction (m)

Greek symbols

γ	Gravity potential (Pa/m)
λ	Latent heat of vaporization (kJ/kmole)
δ	$U_{n+1}-U_n$, Value at time levels
μ	Viscosity (Pa s)
ν_o	Initial Poisson's Ratio
ν_T	Poisson's Ratio temperature dependent factor
ρ	Density (kmole/m^3)
σ_h	Horizontal stress (Pa/m^2)

σ_v	Vertical stress, (Pa/m ²)
τ	Transmissibility, (m ³)
ψ	Geometric mean of mole fraction and mass fraction.

Subscripts

<i>1,2</i>	Direction
<i>c</i>	Conductivity, capillary, component
<i>e</i>	Effective
<i>E</i>	Enthalpy
<i>f, fracture</i>	Pertaining to the fracture
<i>g</i>	Gas
<i>go</i>	Gas in oil
<i>h</i>	Horizontal
<i>i</i>	Component
<i>ip</i>	Injection or Production term
<i>j</i>	Phase
<i>L</i>	Lightest component
<i>Lf</i>	Saturated liquid in the fracture
<i>matrix, m</i>	Matrix
<i>mn</i>	Maltenes now, normalized
<i>mni</i>	Maltenes initially, normalized
<i>o</i>	Upstream weighted value, Oil

<i>ox</i>	Oxygen, or other non-condensilbe gas
<i>pore</i>	Pore
<i>rock, R</i>	Rock
<i>r</i>	Radiation
<i>rea</i>	Reactions
<i>s</i>	Steam
<i>T</i>	Temperature

Chapter 1

Introduction

1.1 Reservoir Simulation

Numerical reservoir simulation provides a means to predict the behaviour of an underground petroleum reservoir and to gain understanding of its complex nature. Little is actually known about a virgin reservoir, except for the few meters around the penetrating wellbores. By producing the reservoir fluids, information can be inferred about the whole reservoir, through history matching with a numerical simulator. Input parameters to the simulator are adjusted until an acceptable fit between the actual production history and simulator production is achieved. The longer the production history, the greater the confidence level in the predictive capability of the simulator. From the fitted parameters, information can be derived about the reservoir process(es).

In order for the simulator to provide meaningful information, it must be reasonably mechanistic. Too simplistic a model will lead to problems in history matching. Too many processes will have to be lumped into too few adjustable parameters. Information about the reservoir, buried in the fitted parameters, may be too difficult to de-convolute to provide any better understanding of the reservoir. On the other hand, too complex a model also leads to history matching problems. With many adjustable parameters there may be multiple solutions for a fit. Also, more preliminary work will be required to develop the necessary input information. Furthermore, the added complexities in the model

will require more time to history match. The optimal model will be the simplest one, which can adequately represent the complexities in the actual reservoir.

1.2 Reservoir Models

The black oil fluid model (three phase, three component, isothermal system) with Darcy flow is the simplest model, and is adequate in representing most reservoirs. Modifications for dual porosity are required when the bulk fluid flow is in fractures. More complex fluid models (compositional) are required when the hydrocarbon phases (oil or condensate and/or gas) cannot be represented by single components. The compositional model requires the simultaneous solution, to a set of conservation equations in finite difference form, coupled with the isothermal thermodynamics. Thermal models are similar to compositional models, with the added complexity of an enthalpy balance and non-isothermal thermodynamics. In cold bitumen reservoirs, fracturing of the matrix occurs to accommodate the injected fluids. Reactions in the thermal reservoir further complicate the situation. For example, the heat from the injected steam thermally cracks the oil. Cracking produces gas which in turn affects the thermodynamics and the oil viscosity. The addition of the reactions and the fracturing to the thermal model results in a very complex system. In order for a thermal simulation to be successful, many of the reservoir parameters must be predefined, and the number of adjustable parameters must be kept to a minimum.

1.3 Computer Time Requirements

Another consideration in reservoir simulation is the amount of computer time required to perform a simulation. A large number of computer runs have to be made in order to history match the actual production. Therefore the simulator must be as efficient as possible, to keep the amount of work done to a minimum. For example, the amount of work that is required for the thermal model increases with the cube of the number of equations per grid block. Therefore the smallest number of components which can adequately represent the system should be used. Fewer grid blocks, of course, result in less time consumption. The bandwidth of the matrix increases with the dimensionality of the simulation, therefore one and two dimensional models should be used whenever possible.

1.4 Gradients, Non-linearities and Grid block Size

With the finite difference solution it is assumed that there are no gradients within a grid block (grid blocks are homogeneous and come to instantaneous thermodynamic equilibrium). Gradients within the reservoir only occur between grid blocks. The validity of this assumption depends upon how well the state variables and the dependent properties are represented by the average values found in a grid block. If the correlation equations (for calculating properties, i.e. viscosity) in terms of the state variables are highly non-linear, smaller grid blocks must be used to ensure that the finite difference

difference solution is a reasonable approximation to reality. In a thermal reservoir there are four types of gradients in state variables which must be accounted for. These are saturation, compositional (mole fractions), temperature and pressure gradients.

The gradients in thermal reservoir simulation are very difficult to model with equilibrium grid blocks. Even with very small grid blocks intra block gradients exist. On injection, the matrix often fractures to accommodate the influx of material which cannot be carried away with Darcy flow. Fracturing of the reservoir is clearly a non-equilibrium process, which results in dispersion of the injection fluid, rather than a frontal advance as in Darcy flow. Other non-equilibrium processes occur when hot gases channel through the reservoir and do not come into thermodynamic equilibrium with the bulk oil. An example of channelling is evident when oxygen is recovered at the producing wells during in-situ combustion projects. Mass and heat transfer effects may actually dominate the processes occurring in the reservoir. Ignoring these processes will not lead to an informative history match.

The aspect ratio and the size of the grid block have a very strong effect on the solution. Often in application the grid blocks are very much larger in one direction than the others. In a system where frontal displacement is the main mechanism, in order to capture the gradient, the grid is refined in the direction of the gradient. For dispersive systems the opposite is true. The greater the length in a given direction the greater the numerical dispersion in that direction.

This dispersion can be used, at least in part, to model fractures (dispersion) which have a specific orientation. On injection, the rate at which the grid block temperature rises is a function of its size. Therefore, the larger the grid blocks the more dispersed the energy is in the reservoir. In multi-gradient systems however, the grid block size is restricted by the sharpest gradient. Therefore, if intended, dispersion in the other variables must be handled in other ways. Also, the use of large grid blocks on production may lead to a poorly defined pressure gradient. It is usually better to define the dispersion in the system with a mechanistic model rather than relying on numerical error to create this effect. Clearly, if all the processes are dispersive, then larger grid blocks can be used. Lower inter grid block gradients allow the use of larger grid blocks. Once the dispersion extent is defined by a model, it is a simple matter to develop a scheme which minimizes the problem size and yet captures the necessary characteristics of the process.

1.5 Fracturing

Hydraulic fracturing of the reservoir occurs when the injected fluids cannot be transported by Darcy flow. The pore pressure builds until the matrix yields to form a fracture. The orientation of the fracture is generally considered to be a function of the rock properties and the local stress fields. Good estimates of the fracture propagation can be found through the use of geo-mechanical models in consolidated reservoirs.

Uncertainties still exist on the exact nature of fracturing in unconsolidated tar sand (uncemented sand). Unlike consolidated reservoirs, where relatively thin cracks form with hydraulic fracturing, large volumes of sand are disrupted by fracturing in unconsolidated sands. Evidence for this is contained in the measurement of surface heaving observed around steam injection plots (Butler 1991).

1.6 Objective of Study

The main thrust of this work is to develop a fracture model which can account for the dispersion of energy in the reservoir (by fracture flow) during steam stimulation. The fracture model will be dynamic and mechanistic in a macroscopic sense. With the dispersion defined with a fracture model, the number of grid blocks necessary for the simulation will be minimized. Computer time usage, thermodynamics, degrees of freedom and formulation of the problem will be discussed in detail as side issues.

The time consumption is an important practical consideration when developing models for thermal simulation. If the numerical model for the fracturing process is to be practical, then the incremental time requirements of the model must be low. If a greater understanding of the fracturing process is to be gained, then the model must be reasonably mechanistic. On the other hand, the mechanism should not be so complex that there are a large number of adjustable parameters. These constraints impose limitations on the fracture

model. The fracture model developed in this work attempts to minimize the adverse impact of these limitations.

Athabasca bitumen is chosen as the oil system to be used in this study. The Athabasca deposits are fairly shallow and extremely viscous (millions of centipoise) in the virgin reservoir. Although these unconsolidated formations are very permeable (1000s of milli-Darcies), and represent a vast resource they have not been exploited to any great extent by in-situ means. This is mainly because of the difficulties in the reduction of the viscosity. However, this bitumen has been studied extensively and a wealth of information on its properties are present in the literature. The availability of this information, as combined with the vastness of the resource, makes this hydrocarbon deposit an attractive choice for study.

Steam flooding of a bitumen reservoir cannot be successful. The bitumen cannot be pushed to the producer because of the high bitumen viscosity. It is necessary to inject steam, then produce the heated bitumen back through the same well. This process is known as the "Huff and Puff" method or cyclic steam injection. Usually a number of cycles are required to drain the reservoir to any extent. This work concentrates on the first cycle.

Chapter 2

Literature Review and Development of Fracturing Concept

2.1 Thermal Reservoir Models, Darcy Flow Only

In general, thermal models require the solution to a number of component balances (see Appendix A), constraint equations, thermodynamic equilibrium equations, and one enthalpy balance. The method of solution of these equations does not vary much. The main difference in solutions is in the arrangement of the equation set.

Coats (1980) developed a simulator for in-situ combustion. The method of solution of the set of equations is fully implicit and fully coupled. Fully implicit means that all the equations are solved simultaneously, by Newton-Raphson and application of constraints. This ensures the most stable solution to the problem possible. Fully coupled means that the thermodynamics properties are completely integrated into the flow equations.

In general, the thermal model consists of N equations where $N=N_c+N_p+2$ and N_c and N_p denote the number of components and the number of phases respectively. The model equations are:

- N_c Component mole balances (see Appendix A)
- 1 Energy balance equation
- 1 Saturation constraint
- N_p Mole fraction constraints

For a four phase system (oil, water, gas and solid coke) involving a two

component oil, hydrocarbon gas, oxygen, water and coke, Coats' simulator requires the matrix solution to a minimum of six equations. The dependent state variables and equilibrium equations are calculated from constraint and correlation equations respectively. Correlations, which are functions of the state variables, are also used to calculate the properties of the fluids and the rock. The six equations required are water mole balance, heavy oil component balance, gas mole balance, light oil mole balance, oxygen balance (or other non-condensable gaseous component) and the enthalpy balance. Since the fourth phase (coke, solid) does not flow, it can be calculated as a constraint equation eliminating two degrees of freedom from the matrix (coke saturation, and the coke primary phase mole fraction). The remaining state variables, minus those eliminated through constraint equations, are aligned opposite the six equations for the Newton-Raphson solution. It is necessary to calculate by Newton-Raphson, 2 saturations, at least one mole fraction in each phase (3 mole fractions), pressure and temperature. Since water is assumed to be immiscible in oil and has a fixed mole fraction of one, one less variable can be solved for. This gives six Newton-Raphson variables, thus the necessity for six equations in the Newton-Raphson solution. If more component equations are present they are aligned with their mole fraction.

The mole fraction of component i in the j th phase is calculated as

$$x_{ij} = K_{ij} * X_i \quad 2.1$$

where K_{ij} is the phase distribution coefficient and X_i is the mole fraction of

component i in component i 's primary or "master" phase. Thus, if the phase is the i th's components master phase $K_{ij} = 1.0$. If the i th component is insoluble in the j th phase then $K_{ij} = 0.0$.

Differentiation of the conservation equations (for the grid block) with respect to the chosen set of primary variables (differentiation variables) leads to the formation of a sub-Jacobian matrix. For a two dimensional system there are 5 sub-Jacobians per grid block. The equation set must be differentiated with respect to the main grid block's and the four interacting grid blocks' primary variable sets. An example of a sub-Jacobian for a set of conservation equations, f_1 to f_6 , is shown below:

$$J = \begin{array}{c} \left| \begin{array}{cccccc} \frac{\partial f_1}{\partial S_w} & \frac{\partial f_1}{\partial S_o} & \frac{\partial f_1}{\partial P} & \frac{\partial f_1}{\partial X_m} & \frac{\partial f_1}{\partial X_{ox}} & \frac{\partial f_1}{\partial T} \\ \frac{\partial f_2}{\partial S_w} & \frac{\partial f_2}{\partial S_o} & \frac{\partial f_2}{\partial P} & \frac{\partial f_2}{\partial X_m} & \frac{\partial f_2}{\partial X_{ox}} & \frac{\partial f_2}{\partial T} \\ \frac{\partial f_3}{\partial S_w} & \frac{\partial f_3}{\partial S_o} & \frac{\partial f_3}{\partial P} & \frac{\partial f_3}{\partial X_m} & \frac{\partial f_3}{\partial X_{ox}} & \frac{\partial f_3}{\partial T} \\ \frac{\partial f_4}{\partial S_w} & \frac{\partial f_4}{\partial S_o} & \frac{\partial f_4}{\partial P} & \frac{\partial f_4}{\partial X_m} & \frac{\partial f_4}{\partial X_{ox}} & \frac{\partial f_4}{\partial T} \\ \frac{\partial f_5}{\partial S_w} & \frac{\partial f_5}{\partial S_o} & \frac{\partial f_5}{\partial P} & \frac{\partial f_5}{\partial X_m} & \frac{\partial f_5}{\partial X_{ox}} & \frac{\partial f_5}{\partial T} \\ \frac{\partial f_6}{\partial S_w} & \frac{\partial f_6}{\partial S_o} & \frac{\partial f_6}{\partial P} & \frac{\partial f_6}{\partial X_m} & \frac{\partial f_6}{\partial X_{ox}} & \frac{\partial f_6}{\partial T} \end{array} \right| \end{array} \quad 2.2$$

The sub-Jacobian matrices (blocks) are placed into the Jacobian for the whole reservoir. The resulting matrix is a penta-diagonal block Jacobian.

The placement of the primary variables opposite the appropriate equation

is an important factor in the solution. The optimum primary variable set satisfies the degrees of freedom and leads to the most diagonally dominate sub-Jacobian possible. The optimum primary variable set (vector) varies depending upon the circumstances experienced in the grid block. Therefore, it is best to change the primary variable set to fit the conditions experienced by the grid block rather than using a fixed primary variable vector. (Also, if a fixed vector is used, then special operations must be carried out to ensure the Jacobian matrix does not become singular.) For the two cases considered by Coats (1980), (gas phase and no gas phase) the primary variable vectors (alignment of primary variables) are shown in Table 2.1. The sub-Jacobian shown above is for the case when gas phase is present.

Table 2.1 Alignment of Conservation Equations with Primary Variables

CONSERVATION EQUATION	GAS PHASE	NO GAS PHASE
f_1 WATER EQUATION	S_w	S_w
f_2 HEAVY OIL COMPONENT EQUATION	S_o	P
f_3 GAS COMPONENT EQUATION	P	X_g
f_4 LIGHT OIL COMPONENT EQUATION	X_m	X_m
f_5 OXYGEN EQUATION	X_{ox}	X_{ox}
f_6 ENTHALPY EQUATION	T	T

Depending upon whether or not a gas phase is present, a specific set of primary variables is aligned opposite a fixed order of equations. It is important that the order of the equations remains fixed so that the derivatives, with

respect to variables of adjacent grid blocks (grid blocks which interact with the centre block), are calculated with the same equations as the centre grid block. This allows an efficient method of calculating the Jacobian and averts confusion concerning placement of terms in the Jacobian. To prevent cross term problems with the equations aligned opposite the pressure variable, Coats sums all the component balance equations and aligns this sum opposite pressure in the Jacobian. Similarly, the components for the oil are summed opposite the oil saturation.

Rubin and Buchanan (1985) developed a general purpose thermal simulator. There is little difference in the basic idea between Coats' model and the model published by them. The main difference is in equation formulation. The constraint equations can be accommodated into the Newton-Raphson set of equations. Ito's (1984) fracturing model of pressure dependent transmissibility multipliers is also included into the simulator. Treatment of the production terms are more advanced than that of Coats' model and efficient equation solvers allow the solutions to practical sized problems.

Brantferger, Pope and Sepehrnoori (1991) described a simulator which uses an equation of state to calculate the thermodynamic properties of the fluid. This ensures consistency and avoids convergence problems with correlations. It is not clear how much time their program requires to perform the Gibbs free energy minimization on a reservoir scale. If this time required is manageable then this method has distinct advantages. Not only are convergence problems

avoided, the forcing function of the minimization may help reduce multiple solution problems.

2.2 Correlations

The body of information on the properties of Athabasca bitumen is large and continues to grow. Correlations and data from the literature allow the development of a properties package that accurately represent the fluids in a bitumen reservoir. Confidence in these correlations eliminates any need to history match the properties of the fluids or the rock properties. Furthermore, the time steps and the number of iterations per cycle are greatly reduced with more consistent correlations.

The book "The Properties of Water and Steam in SI Units", edited by Schmidt (1969), provides a correlation for water in the liquid and gaseous state. This correlation is very accurate (accurate enough for steam tables) for predicting thermodynamic properties of water, and is applicable over a very wide range of temperatures (273.15 to 1000.0 K) and pressures (0.01 to 1000 bar). The error in enthalpy, density, and vapour pressure is less than one percent in the region of application. Since both fluid phases are calculated from the same correlation, consistency within the correlation is ensured.

Xu and Hepler (1990) provide the Henry's constants and infinite dilutions for gases in bitumen (Athabasca and Wolf Lake). The Henry's constants are used to calculate the K (phase distribution coefficients) values for gas in the

bitumen. Also provided are heats of solution. Their data only goes up to 150 degrees C. Since the temperatures reached in the simulator are significantly higher, there will be some error in the fit equations.

Mehrotra and Svrcek (1985) provide the density information data for the bitumen saturated with gas for a number of pure gases. For this work the gas assumed to be dissolved in the oil is ethane. A fit of the data provided, gives the effect of dissolved gas on the density of the bitumen at a given partial pressure of the gas and temperature of the system. Since the information is only for relatively low temperatures (387.15 K), linear extrapolation to higher temperature will result in error.

Mehrotra, Sarkar, and Svrcek (1985) calculated the bitumen density and gas solubility with the Peng Robinson equation of state. Molecular weight and petroleum cuts (fractions) are provided which are necessary for the K-value sliding scale to be described later.

Mehrotra (1992) developed an easily implementable two parameter correlation, which allows the calculation of bitumen viscosity saturated with dissolved gases. Mixing rules for the gas saturated bitumen allow the investigation of the effect of viscosity reduction by gas. Because of the availability of data, for this study, ethane is assumed to be the gas saturating the oil. The bitumen may not be saturated with gas at a given pressure, however it is assumed that correlation is valid for other dissolved mole fractions (mass fractions) other than the saturated case.

Bulter's (1991) book provides most of the remaining properties of the rock and the fluids used in this study. These properties include the thermal conductivity of the matrix, enthalpy of the bitumen and heat capacity of the rock. The correlations were implemented into the simulator in the form used by the original authors. Also this book is used as a general reference on steam stimulation and fracturing.

Belgrave, Moore, Ursenbach, and Bennion (1990) provide the kinetics and stoichiometry for the reactions of Athabasca bitumen. The cracking reactions during steam injection create gas which has an effect on the viscosity of the bitumen and the pressure of the system. The gas produced from the cracking reaction is assumed to have the lumped characteristics of ethane.

Farouq Ali and et al. (Alberta Research Council) (1986) provide the end points of relative permeability curves for bitumen in sand packs. An important, but contentious result, is that the end point saturation does not vary with temperature. This means that the relative permeability curves can be found at a single temperature, and used throughout the range. The residual water saturation is about six percent for all temperatures between 125 °C and 250 °C.

2.3 Pseudo Functions

Pseudo functions are volumetric averages of saturations and relative permeability (Thomas, 1983). If the non-linearities in the conservation equations are small and if there are low gradients, then pseudo functions can

be used to reduce the number of grid block required in a vertical column (direction). Since the finite-difference solution of the reduced system calculates the average saturation in a column of grid blocks, an average relative permeability is used to calculate the flow rate. The pseudo functions' averages are calculated from a simulation run with a refined grid in the vertical direction. The flow in the reduced grid system is matched to the flow of the refined grid system. The new set of relative permeability curves developed are used with the reduced grid system to minimize the work required in the subsequent runs.

2.4 General Reference

Aziz and Settari (1979) provide general information on reservoir simulation. Without the basic principles and knowledge presented in this book, this project would not have been possible. In particular, numerical methods (i.e. D4 ordering) of improving the simulator's performance is acquired from their book.

2.5 Hydraulic Fracturing in Consolidated Sands

Hydraulic fracturing of consolidated sand is usually described by geo-mechanical mechanisms (see Figure 1). The fracture will form perpendicular to the minimum principle stress (Allen and Roberts, 1982). Vertical fractures usually form since the over burden provides the maximum principle stress. Given the Poisson's ratio of the rock, ν , the Young's modulus, E , and the net

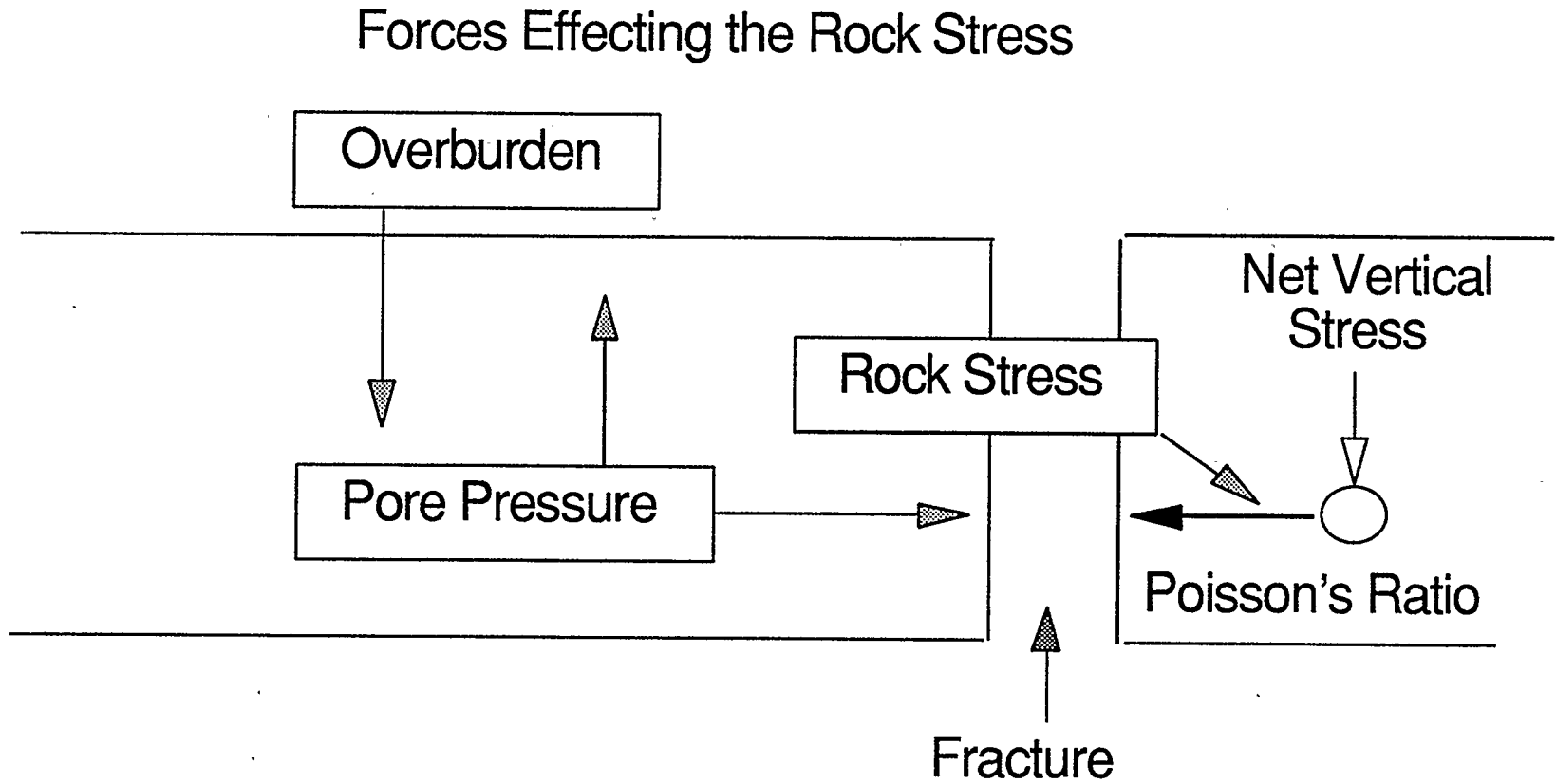


Figure 1 Rock Stress on a Vertical Fracture

horizontal (or vertical) stress, σ , the fracture width can be calculated. The Poisson's ratio is the fraction of the overburden strain transmitted to the horizontal direction. The Young's modulus is the ratio of the stress to the strain. Due to heterogeneity of the reservoir these factors are not well known quantities. However a reasonable estimate of the width can still be found. The fracture width is proportional to (Allen and Roberts, 1982):

$$Width \propto \frac{\sigma}{E} \quad 2.3$$

With the width known, then the conductivity or permeability of the fracture can be estimated, along with the radius of propagation (Settari and Raisbeck, 1981).

The fracture pressure is defined by the force balance in Equation 2.4.

$$P_{fracture} = P_{pore} + P_{stress} \quad 2.4$$

The rock stress is the total stress exerted on the fracture by the rock. Rock stress includes the stress perpendicular to the fracture orientation (effective compressive stress) and the extra stress induced by the fracture width (net fracture pressure). If the viscosity of the injected fluid is low the pressure drop in the fracture is small and the pressure in the fracture is nearly equal to the injection pressure. Given that the fracture pressure is nearly constant, a change in the pore pressure results in the opposite change in the rock stress. In geomechanical models the pore pressure is assumed to be constant, therefore the rock stress is constant.

To calculate the fracture width it is necessary to know the net fracture pressure. It can be estimated from the injection pressure less pore pressure and the effective compressive stress. In the case of a vertical fracture, the net principle stress is the overburden stress less the pore pressure. Allen and Roberts (1982) give the effective compressive horizontal stress, σ_h , as:

2.5

$$\sigma_h = \frac{\nu}{1-\nu}(\sigma_v - P_{pore})$$

where σ_v is the overburden pressure (stress).

In general, to initiate fracturing the pressure must exceed the higher stresses around the well bore. To hold the fracture open after initiation (or to just keep it from closing) the pressure in the fracture must exceed the pore pressure by effective horizontal compressive stress and this is known as the fracture closure or opening pressure. Usually the tensile strength of the rock is small (especially weakly cemented sands) and can be neglected. To propagate the fracture, the pressure in the fracture must exceed the rock closure pressure by the net fracture pressure and the pressure drop in the fracture due to the resistances in the fracture. Increasing the pressure in the fracture (holding the pore and the rock closing pressure constant) increases the width of the fracture, by increasing the net fracture pressure. Wider fractures provide less resistance to flow.

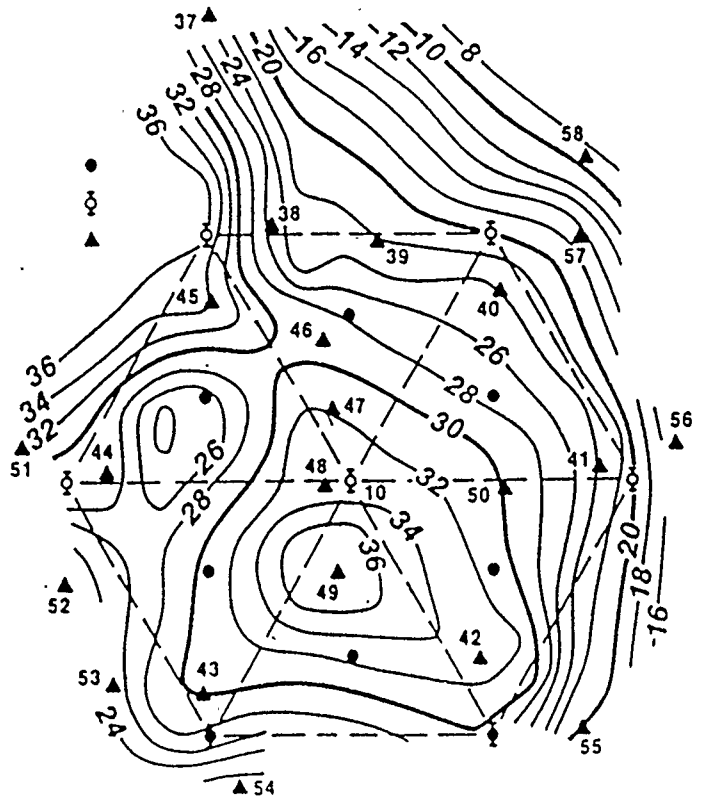
In consolidated sands, as the temperature increases in the grid block the matrix loses some of its original compressive strength (Allen and Roberts,

1982). The loss in strength causes the Poisson's ratio to increase. This puts more of the net overburden pressure onto the fracture. Since rock opening pressure increases, the net fracture pressure must increase to maintain the width. However, the Young's modulus decreases requiring less pressure in the fracture to maintain the width. The lower resistance in the fracture will allow more flow in that direction. The effects of the changes in the Young's Modulus and the Poisson's Ratio tend to cancel out when determining the fracture path. To what degree is unknown.

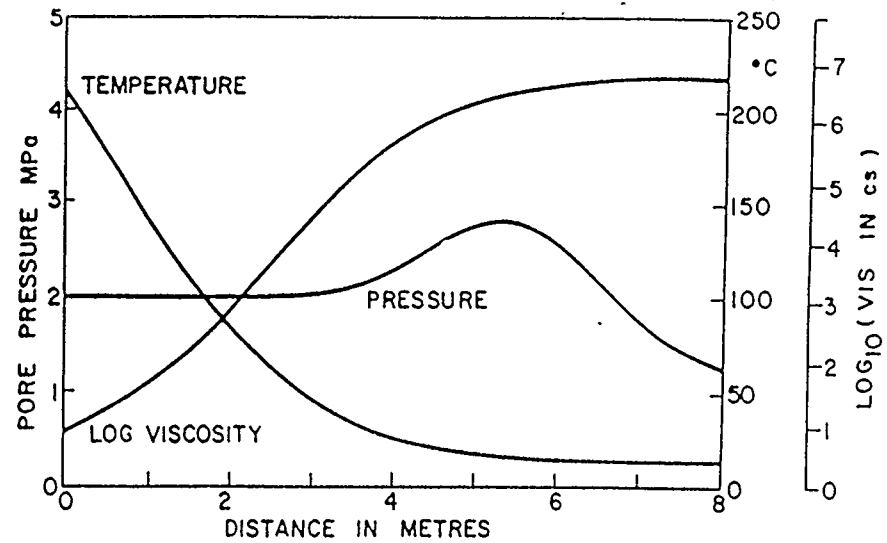
2.6 The Nature of Fracturing in Oil Sands

Thermal hydraulic fracturing of an unconsolidated reservoir is not well understood. In unconsolidated reservoirs the fracture pattern is quite complex (Settari and Raisbeck, 1981). Changes in the properties of the rock and the pore pressure increase the complexity of the problem. In consolidated rock, thin fractures are formed which propagate in the direction perpendicular to the plane of minimum stress. Settari and Raisbeck (1981) have developed a model to accommodate this phenomena. The model for formation of these single fractures is based on the properties of the rock (geomechanical model). In unconsolidated material however, the fracturing is probably distributed rather than forming a single channel. Strong evidence for this is the heaving of the surface about steam injector wells (Figure 2a) (Butler 1991).

Examination of the literature provides some understanding of the steam



a) Surface Heave about a Steam Injector, Hundredth's of a foot (Butler, 1991)



b) Effect of Heating after 50 days On Pore Pressure (Butler, 1986)

Figure 2 Surface Heave (a) and Pore Pressure (b)

fracturing process in oil sands. Ideas inferred from these previous works are employed to develop a new fracturing concept. The following subsections highlight important principles (and evidence) necessary for the development of this concept.

2.6.1 Matrix Disruption

Butler (1986) modelled the thermal expansion of tar sands, due to heat conduction into the reservoir matrix. He showed that the pore pressure can be higher than the pressure of the injected steam because of the thermal expansion of the fluids. Figure 2b shows the pressure in the rock matrix as a function of the distance to the steam source after 50 days. The large bump (jump in pressure) in the pressure profile (at 6 meters) is thought to disrupt the matrix. Even with the steam pressure below the fracture pressure, disruption (movement of the individual sand grains from their original tightly packed formation) of the rock matrix can occur. Disruption of the matrix results in porosity and permeability changes in the matrix which never return to their original values (hysteresis). Disruption and the thermal expansion of the reservoir also explain the surface heave about steam injectors. The extent and rate at which the disruption of the matrix occurs, will increase if an immobile gas phase is present in the matrix or if there is convection of fracture fluids into the matrix. The thermal expansion of a gas is high, which will result in greater disruption of the matrix with the conduction of heat from the fracture.

Convection of fluids into the matrix (i.e. condensed steam) will carry thermal energy from the fracture, into the matrix at a higher rate.

For a steady state fracture to be maintained, the fracture pressure must be equal to the rock stress plus the pore pressure (Equation 2.4). Clearly the pore pressure cannot be greater than the fracture pressure or the fracture will close. However, in the matrix very near the fracture's wall (a centimetre or two into the matrix from the fracture) the pore pressure can rise rapidly to the fracture pressure. The actual fracture is therefore not supported by any rock stress. Geo-mechanical models are based on the assumption that the rock properties (i.e. Young's modulus, horizontal compressive stress) are dominant factors in determining the nature of the fracture. Obviously this is not always the case with steam fracturing. These geo-mechanical models will not work in unconsolidated sands at higher temperatures, although the fractures initially do form in this fashion when the pore pressure is still low.

Along with changes in the rock stress due to temperature, Butler's (1986) work gives a mechanism for the formation of a distributed fracture system. As the pore pressure increases the fracture finds it more difficult to maintain its path. Since the Poisson's ratio also increases with temperature, the resistance to the flow in the fracture increases. Finally the fracture closes and the steam finds a new path where the pore and the rock stress are not so high (a cooler part of reservoir).

2.6.2 Hydraulic Fracturing of Unconsolidated Oil Sands

Settari and Raisbeck (1981) studied the fracturing in an unconsolidated Cold Lake reservoir. A geo-mechanical model was developed to analyze cyclic steam stimulation in oil sands above the fracture pressure. A numerical model was formulated that simultaneously describes the fracturing process and the reservoir behaviour for different types of fracture geometry. The model was used to study the performance expected for different fracture types. The comparison of the model results with data from first cycle steam injection shows good agreement for a single vertical fracture configuration.

A non-vertical fracture orientation usually indicates the Poisson's ratio is high (but unknown). The problem is to find an appropriate Poisson's ratio, Young's modulus, and the fracture orientation, which allow the calculation of the rock stress. In consolidated reservoirs the Young's modulus decreases and the Poisson's ratio increases with increasing temperature (Allen and Roberts, 1982). These effects are probably magnified in unconsolidated reservoirs where the matrix disrupts. Therefore the degree of uncertainty in these factors increases in an unconsolidated sand.

2.6.3 Other Thermal Fracturing Models

In view of the complexities in hydraulic steam fracturing in unconsolidated sands, there are a number of different methods of describing these fractures in the literature, other than geo-mechanical means. One is the

hot streak method, which describes the fracture as a narrow channel of very high permeability. This permeability to the injected fluid is provided by giving the zone a high initial water or gas saturation. Darcy flow follows the path of least resistance, therefore injected fluids will flow along these preset paths.

The orientation of the fracture can be vertical or horizontal. Dispersion of the fracture is further enhanced by the aspect ratio of the grid blocks. There are three major problems with the hot streak method. Firstly, the orientation of the fracture is fixed. The location and the fracture properties must be known prior to the simulation. Secondly, the fracture does not close on production. This will lead to history matching problems in cyclic steam projects. Thirdly, the rock stress in the single fracture is completely ignored.

Another method used when the reservoir does not fracture in a predominant direction, is to increase the compressibility of the reservoir. This can be done by the addition of gas or by making the rock highly compressible. These factors allow Darcy flow of the injected fluid through the matrix without the pressure in the system becoming extremely high. The main problem with compressibility models is that the concept of heat dispersion into the reservoir is lost. Equilibrium grid blocks cause frontal movement of the energy in the reservoir, rather than dispersive movement expected with fracturing.

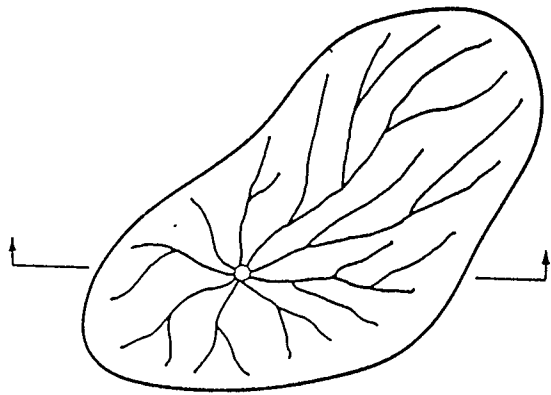
2.6.4 Ito's (1984) Dispersion Model

Fracturing produces heat dispersion in the reservoir. To account for this,

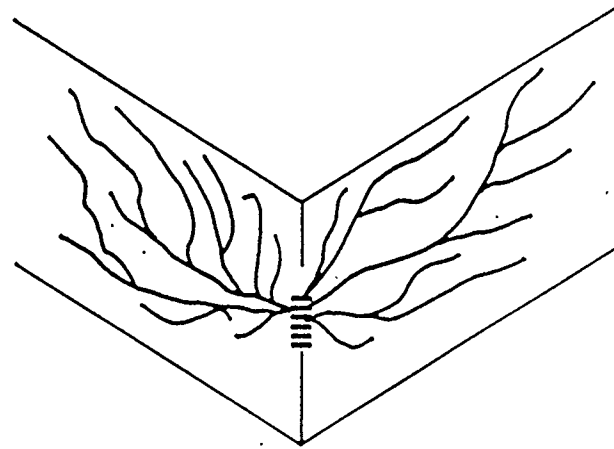
Ito (1984) developed his micro-channelling concept (Figure 3). Micro-channelling assumes fracturing is distributed (i.e. injected energy and mass flows in all directions). This means that relatively large volumes of the reservoir rock are contacted with the steam and an uniform property distribution is produced in the fractured zone.

Ito's fracturing model is a macroscopic approach to the problem. The fracture model consists of super upstream weighted enthalpy and transmissibility multipliers. The transmissibility multipliers are pressure dependent factors (i.e. as the pressure goes up the factor increases up to a terminal value). The multipliers are used to increase the permeability of the matrix under Darcy flow to represent the flow in the fractures. In order to represent the steam bypassing a grid block, Ito's fracturing model multiplies the upstream equilibrium enthalpy by a pressure dependent factor (super upstream weighted). Super upstream weighting of the enthalpy flow allows the simulation of steam flow with liquid water. The multiplication factors are history match parameters. This model can be classified as dispersive, which correctly simulates the effect of the fractures carrying heat and mass further into the reservoir than is possible with Darcy flow.

Ito obtained good history matches with his sand deformation model. A number of factors previously difficult to fit were now much closer to field obtained values. For this reason, the method has become industry standard in Alberta oil sands. However the history matches are not perfect. Production



Top View



Side view .

Figure 3 Ito's Fracturing Concept

pressures of the model are significantly higher than those in the reservoir.

Although good history matches can be obtained with Ito's model, there are a number of problems with it. Most of these problems become apparent when a gas phase appears. Firstly, the model suffers from numerical difficulties. The multiplication factors for the enthalpy and the mass flow in the matrix lead to thermodynamic inconsistencies in the solution. The thermodynamic inconsistencies cause the simulator to perform poorly. Secondly, the upstream grid block is at equilibrium, therefore the multiplication of permeability results in the flow of the wrong components onto the next grid block. The temperature of the matrix is at a significantly lower temperature than the steam in the fracture. At lower temperatures, the equilibrium mole fractions in the gas phase are out of proportion with the mole fractions of the fracture stream. As a result, Ito's fracturing model leads to excessive gas flow. Also, the multiplication of the liquid water flow rate, to simulate steam flow, does not allow for the density effects to be accounted for in the fractures. Thirdly, the fracture flow is dependent on the relative permeability of liquid water in the matrix. In reality the flow of steam in the fractures has little to do with the flow of liquid water in the matrix. This may cause history matching problems. Finally, Ito ignores the rock stress and matches the pore pressure to the injection pressure. This leads to a high pore pressure in the model. The matched relative permeabilities will not be representative of the reservoir. The production pressures will also be too high. Furthermore, the lack of a

mechanism provides no insight into the fracturing process.

2.6.5 Review of In-situ Pilots In Athabasca Tar Sands and Implication of Data

The tensile strength of the unconsolidated oil sand is low (Settari and Raisbeck, 1981). The sand can be easily broken apart by unbalanced forces. In the reservoir, with the net vertical stress acting as the normal force, frictional forces between the angular sand grains (Butler, 1991) are significant. The high relief of the oil sand along the banks of the Athabasca river indicates the frictional forces are matching the horizontal stresses (i.e. tectonic and the horizontal compressive stress (Equation 2.5)). Since the frictional force cannot be high (some small fraction of the normal force) the horizontal stresses must be low. If the horizontal stresses are low, then Poisson's ratio must be low. This conjecture is supported by the low value of Poisson's ratio (0.2) found by Settari and Raisbeck (1981).

If the tectonic stresses are low then overburden supplies the principle stress. Even with disruption, it is likely that the highly angular sand will be able to maintain a relatively low Poisson's ratio. A low Poisson's ratio means that the horizontal stress is less than the vertical stress. Therefore, it is believed that the fracture orientation is primarily vertical. (An exception has to be made for very shallow reservoirs where it is easier to lift the overburden than it is to compress the rock).

Redford (1986) reviews the many in-situ pilots which have been

attempted in Athabasca bitumen deposits, plus a number of pertinent pilots from related deposits. In general the pilots in the Athabasca bitumen deposits have not been commercially successful. Problems with sand production and low oil to steam ratios appear to be common.

The sand production is further evidence of the matrix disruption. In the original formation the angular sand grains hold together giving the formation surprisingly large compressive strength (Settari and Raisbeck, 1981). Once disrupted by steam injection, the sand grains of the matrix are not arranged in the tight packing of the original formation. Some of the compressive strength of the formation is lost and the Poisson's ratio increases. As a result the formation slumps and the sand production occurs.

The fracturing of the Athabasca deposits has lead to a number of results (Redford, 1986). Firstly, with steam injection, operating conditions indicate that vertical fractures form initially but then they become horizontal. This indicates that the changes in the pore pressure and the rock properties have an effect on the path of the fractures.

Secondly, vertical fractures always form when water is injected but if steam is injected eventually horizontal fractures form. The density of the injected fluid must have a large effect on the fracture path. Also it can be concluded that higher temperatures cause the formation of the horizontal fractures. The formation of apparent horizontal fractures is likely a combination of both the temperature and density effects.

Thirdly, the formation of horizontal fractures seem to be common in shallower reservoirs. Horizontal fractures are usually attributed to a high Poisson's ratio or higher horizontal stress than the vertical stress. In Athabasca tar sand neither of these is the case. It is more likely that the horizontal character observed in these reservoirs is due to the rise in the pore pressure. The pore pressure in a virgin reservoir can be estimated to be one half the overburden pressure (the density of water is about one half that of the overburden matrix). In shallower reservoirs, smaller increases in the pore pressure are required to reach the overburden pressure. From Equation 2.5, once the overburden pressure is reached, the compressive horizontal stress becomes zero. The pressure in the fracture is the same as the overburden stress, and the fracture appears to be horizontal. However, the fracture orientation may not be horizontal. The low rock stress in the formation can lead to any orientation of the fractures. In any case, the path of the fracture will be dominated by the pore pressure.

Finally, others have found that vertical fractures formed, with breakthrough at the top of the formation even though the injection was at the bottom of the formation (Redford, 1986). This clearly indicates that the fractures rise up in the formation. Modelling the gravity override of the fractures is an important factor in the success of the simulation. The degree of the gravity override will influence the distribution of the heat in the reservoir.

2.7 Fracturing Concept

Settari and Raisbeck (1981) found that in deeper reservoirs, the formation of a single vertical fracture best describes the field experience. If a single vertical fracture forms, then it is unlikely that the concentric surface heave about the injector would be observed. A single fracture can only explain the concentric surface heave if the fracture is horizontal. Only one fracturing model can simultaneously allow for the formation of a single vertical fracture and explain the surface heave. Initially a single vertical fracture forms, but it closes due to the increase in the resistances as the matrix in the local area of the fracture is heated. Then a new vertical fracture forms which also eventually closes. Overtime this continual opening and closing propagates fractures in all directions from the injector. Relative to the injection period the opening and closing of the fracture is believed to be rapid. Rapid changes in the local properties of the rock (i.e. increase in Poisson's ratio) and the fluid about the fracture (i.e. pore pressure), result in rapid changes in the resistances in the fracture. The increases in resistances force the fracture to constantly change its path. The net result is the fractured flow which is distributed about the injector (see Figure 4, top view). This hypothesis is the basis for the fracture model to be developed in this work.

The overburden provides the principle stress. Since Alberta oil sands are highly angular, it can be inferred that the Poisson's ratio will never reach the maximum value of 0.5 (0.5 is the same Poisson's ratio for a liquid (Butler,

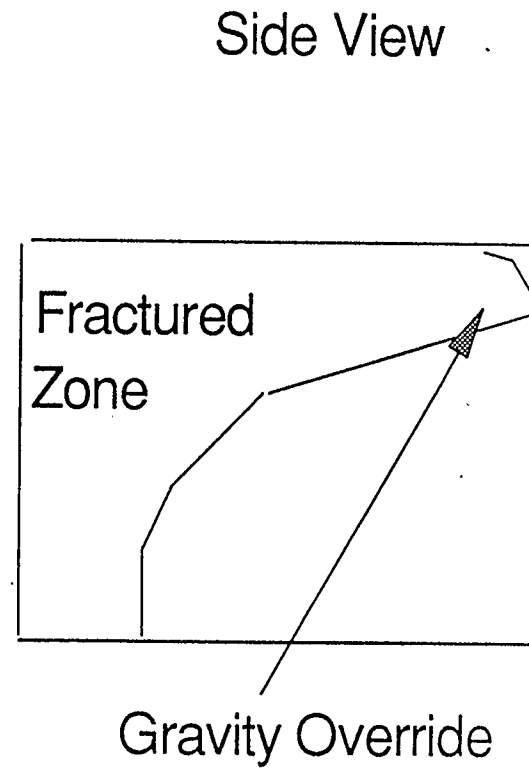
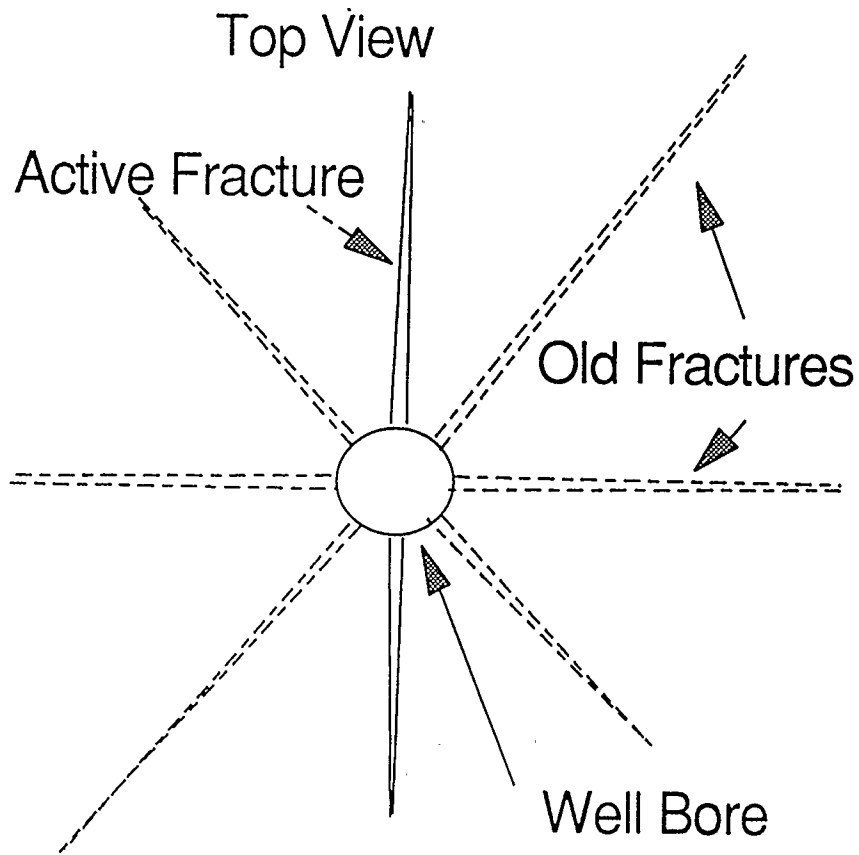


Figure 4 Fracturing Concept

1991)). In other words, the principle stress on the fracture will never be a horizontal stress. Therefore it is speculated that vertical fractures will always form. The horizontal nature of the fractures, exhibited by shallow reservoirs is believed to be a result of high pore pressure.

In addition to the distributed nature of the fracturing in the horizontal direction, the distribution of the steam in the vertical direction must be considered. The information inferred from the work of Redford (1986) gives some insight into the nature of flow in the vertical direction. It is theorized that gravity effects result in the fractures overriding the formation (see Figure 4, side view). Lower pore pressure (due to the weight of the fluids in the matrix) in the vertical direction results in lower resistance in that direction. Furthermore, higher pore pressure requires more energy to propagate the fracture tip (more work is done against a higher pressure). Therefore more flow occurs in the vertical direction. The pore pressure gravity override is reinforced by the lower rock stress in the vertical direction. The effect of the rock stress is somewhat dependent on the pore pressure. Increases in the pore pressure reduces the influence of the rock stress. A complete discussion of the gravity override is provided in the next Chapter (Section 3.4.1.2).

As stated previously when discussing consolidated reservoirs, increases in temperature causes the Poisson's ratio to increase and Young's modulus to decrease (Allen and Roberts, 1982). Increases in the Poisson's ratio increases the pressure on the fracture (increasing resistance in the fracture). A decrease

in the Young's modulus will decrease the resistance in the fracture. The net effect of these factors is believed to be dependent on the depth of the reservoir. Their influence is expected to have a large effect on the gravity override of the fractures. The disrupting fracture walls will cause increased roughness of the fracture walls and cause sand to fall into the fracture. Therefore, it is likely that hotter fracture walls will result in greater resistances to the flow.

Chapter 3

The Simulator

3.1 Overview

If the non-linearities in the conservation equations are small and there are low gradients (saturation, mole fraction, pressure and temperature gradients) in the vertical direction, then pseudo functions can be used to reduce the number grid blocks required. With Darcy flow in a thermal reservoir it is not possible to apply pseudo functions. The non-linearities and the gradients are far too high. Pseudo functions will work in a thermal reservoir, only if the temperature and pressure of the system are fairly uniform. This happens when an unconsolidated bitumen reservoir undergoes fracturing.

A number of special conditions occur in the fracturing zone of an unconsolidated bitumen reservoir. Firstly, the fracturing is distributed. Relatively large amounts of the reservoir are contacted with the steam. This results in a uniform property distribution in the fracture zone. Secondly, the bitumen does not move in the horizontal direction at high rates. This leads to fairly low saturation gradients. High bitumen viscosity and low inter grid pressure drop do not allow the bitumen to move. Also, the high bitumen viscosity allows the formation of fractures. The bitumen cannot flow out of the way fast enough to accommodate the steam flow rate. Thirdly, there are only small gradients in the steam carrying fracture. Naturally fractured reservoirs have a saturation gradient in the fracture, which can be the determining factor

in grid sizing. Due to the small fracture volume, the dynamics in the fracture saturation gradient is fast and hence require smaller grid blocks. However, the fast dynamics of steam fracture (without saturation gradients) leads to rapid development of constant properties within the whole fracture. Therefore the size of the grid blocks is not limited by the fracture dynamics. These properties of the fracturing allow the application of larger grid blocks to simulate the unconsolidated bitumen reservoir.

The starting point for this work is a two dimensional thermal simulator based on the work of Coats (1980). The time requirements of this original simulator are rather excessive (Appendix D). In order to boost the speed of the simulator, some work is required to decrease the time to perform a Newton-Raphson cycle and to increase the time stepping radius of convergence.

Coats' formulation is improved to handle steam injection into Athabasca bitumen. The equation set of this thermal simulator is dynamic. There are different equation sets to be solved in different grid blocks at different times because of phase changes and component disappearances. Re-formulation of the equation set is required to enhance the performance of the simulator. Also a mechanistic model for the fracturing of the reservoir by the injected steam is introduced. The following text of this chapter is broken into three sections, numerical, formulation, and fracturing to provide details of the work in each of these areas. However, the main focus of the chapter is the development of the dynamic fracturing numerical model.

3.2 Numerical

3.2.1 Equation Set

The thermal model consists of N_c component balances, one enthalpy balance, equilibrium equations and N_p+1 constraint equations, where N_c is the number of components in the system and N_p is the number of phases present. The equilibrium values (K values, phase distribution coefficients) are calculated from correlations as functions of the state variables. Therefore the equilibrium equations can be eliminated from the Newton-Raphson set. The application of conservation of mass and energy around an infinitesimal volume leads to partial differential equations in space and time of the form:

3.1

$$IN - OUT + GENERATION = ACCUMULATION$$

These equations are converted to algebraic equations through the application of finite-differences. The details of the derivation of the component conservation equation(s) is given in Appendix A.

The finite-difference algebraic equations from the thermal problem are coupled, and are very nonlinear. The non-linearities in this dynamic system result in a slow convergence to the time step solution. Sequential and/or explicit methods can lead to faster iteration times, but require extremely small time steps for numerical stability. It is generally accepted that the fully implicit method (Newton-Raphson) is more robust and faster in the long run.

The Newton-Raphson set of equations is made up of the conservation

equations and sometimes includes constraint equations. Each of the algebraic equations is differentiated with respect to each primary variable, holding all other variables constant (partial derivatives). The matrix produced by this process is the Jacobian. The Jacobian matrix is essentially a linearized form of the non-linear algebraic equations about the previous iterative step. This linear set of equations can be solved by a matrix solver. In general, the N_c+1 primary variables are solved directly from the matrix solution, while N_p+1 variables are found through the application of constraints.

The Jacobian matrix, required for the Newton-Raphson method, is poorly conditioned because of the high degree of coupling of the equations. Special considerations must be given to the method of solution of the matrix. Setting up and solving the Jacobian matrix is very time consuming. Therefore, the most efficient algorithms possible must be used in the simulator.

Little can be done in decreasing the amount of time required to calculate the numerical Jacobian matrix. Updating the Jacobian requires the calculation of every numerical derivative in the matrix. The use of approximate updating procedures, such as Broyden's method (Burden et al., 1981), are not possible because of the non-linearities and formulation changes. It is, however, possible to make a far better guess at the solution through linear extrapolation of the previous time step increments in the state variables. As long as there is no change in the primary variable set (see Table 2.1), there is a significant increase in the maximum time step and the number of iterations per time step

is significantly reduced. Damping of the matrix solution, by truncating the changes in the primary state variables to a preset maximum value, eliminates serious problems associated with switching to an alternate primary variable set.

3.2.2 Matrix Solution

To reduce the amount of time required by each Newton-Raphson cycle, the matrix must be solved as efficiently as possible. The size of the matrix band for a two dimensional system is calculated as $(2*N_y+1)*N_{eq}*N_x*N_{eq}$, where N_y and N_x are the number of grid blocks in the y and x directions respectively, and N_{eq} is the number of equations per grid block. The factor $(2*N_y+1)*N_{eq}$ is the bandwidth of the matrix. Usually the matrix is ordered in a fashion to make N_y as small as possible to reduce the bandwidth. This is known as natural grid ordering (see Figure 5).

A general direct matrix solver for banded matrices, Gband (Aziz and Settari, 1979) is the normal method of solving the matrix. Gband is Gaussian elimination that only operates within the bandwidth and does not operate on the zeros in the corners. However, the matrix to be solved can become very large therefore even more efficient methods of solving the matrix are necessary.

Iterative techniques for these ill-conditioned matrices involve partial LU decomposition and preconditioners in order to make the system of equations convergent. Even when the matrix is convergent, the accuracy of the solution has to be evaluated. Due to large tolerances in the convergence criteria and

Natural Grid Ordering

1	4	7	10
2	5	8	11
3	6	9	12

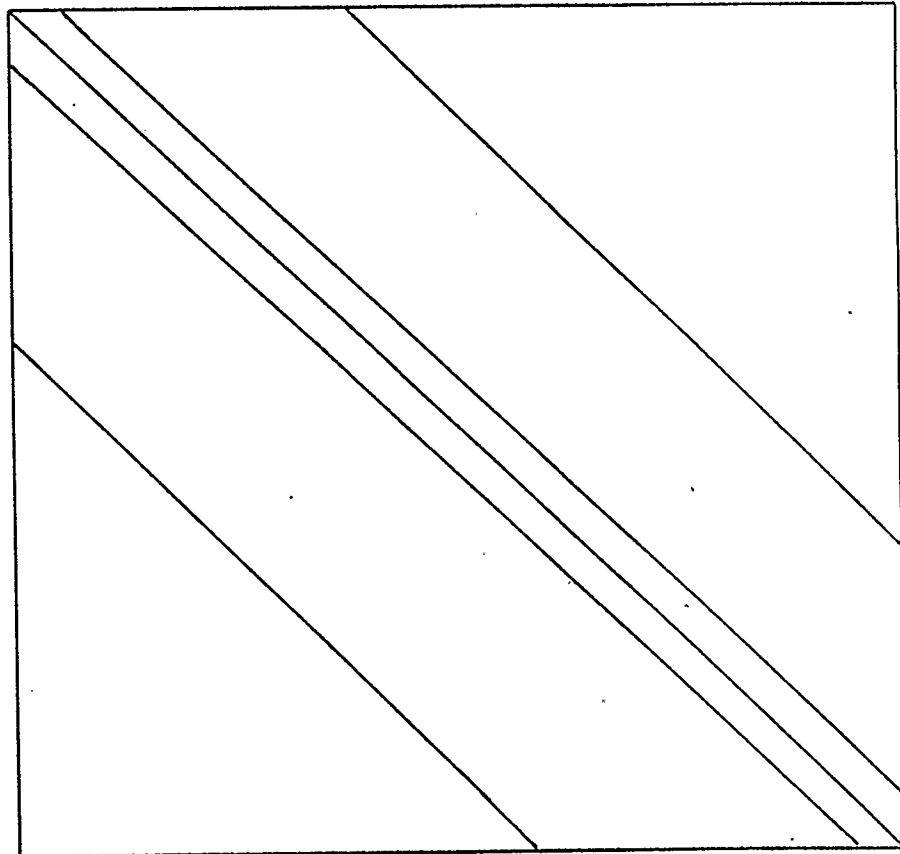


Figure 5

to the poorly conditioned matrix, the solver can converge on erroneous solutions. Furthermore, it is necessary to know a priori how many extra bands (amount of decomposition) are required to make the system diagonally dominant. In the case where the matrix is very ill-conditioned (live oil systems), the amount of work required to perform the decomposition is formidable. However, as the size of the problem increases, the need for iterative techniques becomes clear. This study is confined to 2-D small grid systems (less than 100 grid blocks). An efficient direct method is used, since in the long run it is faster for these small problems. Another advantage of direct methods is that convergence problems of the Newton-Raphson step are more easily identified.

Whether the matrix solution method is iterative or by direct methods, D4 ordering (Figure 6) of the matrix has advantages. This reordering expands the bandwidth out until the off diagonal elements are pushed into the non-diagonal quadrants. This makes the system more convergent for iterative methods. For direct methods, D4 ordering can greatly reduce the amount of work a matrix solver has to do. Only the lower left quadrant has to undergo full Gaussian elimination. An increase of speed of four times can be realized for a large point matrix which arises from a square grid system. Block matrices cannot be solved as efficiently, but a large increase in speed can still be realized through the use of D4 ordering.

The Jacobian matrix for thermal problems has a large number of zeros within the band. With a scalar machine it is very efficient to eliminate these

D4 Grid Ordering

1	7	2	9
8	3	10	5
4	11	6	12

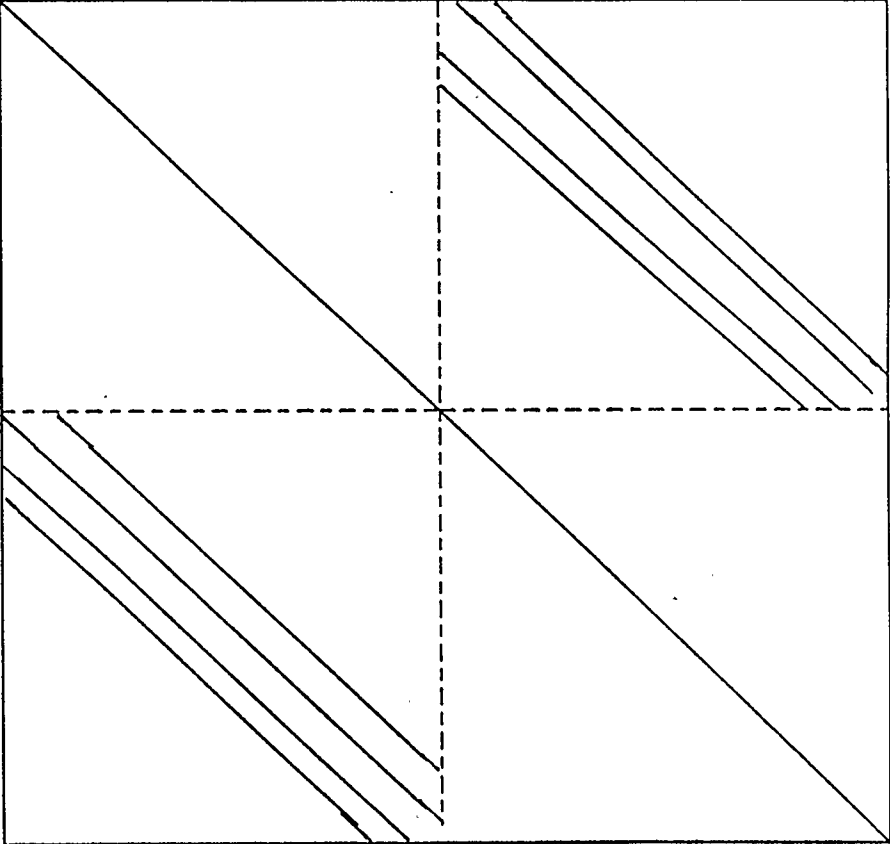


Figure 6

zeros by the use of column pointers. Storage can be reduced significantly if only non-zeros are stored. Furthermore, by only operating on the non-zeros within a row, the number of calculations can be greatly reduced. After scaling, it is often found that certain elements of the matrix are insignificant, and can be approximated with zero. These terms can also be eliminated, further increasing the speed of the solver.

3.3 Formulation

Athabasca bitumen is very viscous at reservoir temperatures. The reduction of the viscosity to a producible level requires the application of heat. Steam is usually the medium for heat transfer to the reservoir. The bitumen viscosity can also be reduced by the addition of a soluble gas, which is sometimes injected along with the steam.

Often, in steam simulations the fluid models are simplified to increase the numerical performance of the simulator. Usually the gas component is considered to be non-condensable or the gas phase is prevented from forming. This has to be done in most cases to minimize the enormous size of practical problems. These simplifications to the fluid models, while hitting on the most important aspects of the reservoir, leave out some points which may be significant. To determine if these aspects are significant, it is necessary to run sensitivity studies. One such point is the inclusion of a soluble gas into the system. Light hydrocarbons are usually present in most bitumen and have a

strong effect on the pressure transients. Furthermore, the thermal cracking reactions produce gas. The inclusion of gas is also necessary for the simulation of the improvement in oil recovery due to the addition of a bitumen soluble gas. In order to do this, the Coats' formulation (1980) has to be improved to handle the gas component properly. The introduction of the gas component, along with the cracking reaction, results in a highly coupled equation set. Although this coupling causes numerical problems, it is felt that for this research these aspects should be included.

Athabasca bitumen is usually divided into pseudo components (maltenes and asphaltenes). Maltenes are long chained saturated hydrocarbons (pentane soluble) while asphaltenes are complex aromatic compounds. These groups behave differently in chemical reactions (Belgrave et. al., 1990). Separating (cutting) the bitumen into four maltenes components and one asphaltenes component can provide reasonable thermodynamic properties when calculated with an equation of state (Mehrotra, Mallika and Svrcek, 1985). However, using that many cuts would require a great deal of computer time. Furthermore, there is no information in the literature on the thermal cracking behaviour of these individual cuts. To save computer time and to work within the information provided, the bitumen is divided into only two cuts, maltenes and asphaltenes.

When applied to bitumen, Coats' formulation (1980) has a number of problems. Most of these can be handled by reformulation and other techniques which are described below.

3.3.1 Absence of Oxygen or Other Non-Condensable Gas Component(s)

Coats' formulation is for in-situ combustion. The application of this model to steam simulation requires some adjustment. It is observed that once the non-condensable gas component disappears, the hydrocarbon mole fraction (X_g) drifts about. Small changes in the shifts (the small amounts added or subtracted from the primary variables to calculate the numerical derivatives) result in significant differences in the solution. It is suspected that the conservation equations are weak functions of the gas mole fraction, therefore the conservation equations can be satisfied with the wrong gas component mole fraction. Whatever the case may be, the problem is solved by moving the gas phase constraint equation into the Newton-Raphson set of equations. As soon as the non-condensable gas disappears, on the next iterative step the non-condensable gas component balance is replaced by the gas phase constraint equation. The primary variable set or vector (see table 2.1) is modified so that gas component mole fraction is a primary variable (X_{ox} is replaced with X_g). The constraint equation is a very strong function of the gas phase mole fraction, thus the above problem is eliminated. This formulation is essentially the same as the Computer Modelling Group's (1984) formulation, for this type of system.

3.3.2 Asphaltenes and Maltenes Component Balance Dependencies

The asphaltenes and the maltenes component balances are not always linearly independent. Each component balance is made up of three elements

(hydrodynamics, reactions and thermodynamics). Unless one of these elements is different, the equations are linearly dependent. The asphaltenes and maltenes cuts (petroleum fractions) of bitumen are so heavy that they are both non-volatile. This means they behave the same thermodynamically and their flow rates are proportionally the same. The only element which is different is reaction rates, which keep the two mole balances slightly linearly independent. Therefore, it is necessary to include both component balances in the Newton-Raphson set. Once the temperature is high enough, the bitumen starts to flow and the reaction rates become insignificant in comparison to the flow term. As a result, singularities can occur, so the simulator is forced to take very small time steps or fails completely.

The bitumen is actually a continuum of hydrocarbons of varying molecular weights. The lighter ends of this continuum will result in some vapour pressure even at moderate temperatures. If a gas phase exists in the grid block, then some of the singularities can be prevented by calculating an integrated average of volatility of the cut. In order to accomplish this, the maltenes are put on a sliding scale. It is assumed the maltenes cut is made up of four pseudo components (Mehrotra, Mallika, and Svrcek, 1985). Any deviation from the maltenes initial mole fraction (corrected for the gas mole fraction) is assumed to occur in the most volatile of the pseudo components remaining. This allows the calculation of an effective average K value for the maltenes, which is not zero. Reid et al. (1977) provides the correlations of the

K-value for each cut based on its molecular weight. Details of this method are provided in Appendix B.

The sliding scale method solves most of the problems with the interdependence of these equations on the first steam cycle. Essentially the method allows the simulation of a number of maltenes sub-components with a single equation. Not only is this method important to the maximum time step, it is also important to the iteration speed of the simulator.

3.3.3 Absence of the Gas Component.

A light gas component is easily stripped from a grid block with the injection of steam. The loss of the gas component results in the loss of two degrees of freedom. Without other volatile components the pressure of the system is only a thermodynamic function of temperature (vapour pressure of water). The pressure is not dependent on the upon the hydrodynamics, since the water vapour pressure is not a function of the amount of liquid water in the system (as long there is some liquid water). Under these circumstances the gas component balance equation and the gas constraint equation can be deleted from the Jacobian. Pressure is then calculated from the vapour pressure curve of water as a function of temperature.

There is a problem, however, with deleting the gas component balance equation. The reactions produce gas and gas flows into the grid block from other sources. Therefore, it is necessary to determine a point when the

formation and the injection of gas are significant, to warrant bringing back the component balance. This is actually a difficult problem to solve. In order to circumvent this problem, the gas is also put on a sliding scale.

The sliding scale for the gas is based on the initial mole fraction of the gas in the oil phase. The light hydrocarbons present in a reservoir are more likely to be a continuum of the homologous series than to be a single component. Given the distribution of the lighter hydrocarbons in the bitumen, an estimate of the volatility can be found. The lower the amount of gas in the oil phase, the heavier its carbon number is assumed to be. Details of the method are provided in Appendix C.

3.3.4 Liquid Water Disappearance

When the liquid water phase disappears, there is no change in the degrees of freedom. It is not necessary to calculate the saturation of water, but the mole fraction of the water in the gas phase must be calculated. Pressure is aligned opposite the water mole balance. The gas constraint equation, if present, is removed from the Newton-Raphson set. The gas component primary mole fraction is aligned with the gas conservation equation. The water mole fraction is found from the (gas phase) thermodynamic constraint.

3.3.5 Thermodynamic Consistency

Correlations are implemented in the form presented by their authors.

When the reference only presented data, the data was fit to an equation form which seemed to give the best fit (these correlations are shown in the appendices, Chapter 4 or are referred to in the literature review). A few of these correlations are sometimes used outside their reported limits. However, in the absence of better correlations they were used after checking that they do not lead to non physical values when employed beyond the specified range.

Consistency between the enthalpy flow and mass flow is very important if a solution is to be found in a reasonable time step. All the state variables should move in the direction of the global minimum solution. When the guess is far away from the solution, there can be difficulties in the primary variables finding the right direction to move. There are local minima (and probably maxima) in which a variable can get stuck and the slope of the function may be zero (horizontal). Consistency in the correlation removes some of these local minimums and gives definition to the slope.

The use of an equation of state would ensure thermodynamic consistency. Also, the forcing function of the minimization may help eliminate problems with local minimums. However, the time required to perform the thermodynamic calculation may be too formidable on a reservoir scale. For this reason, it was felt that it was best to try and develop a consistent set of correlations.

Most of the energy in the reservoir is carried by the water. Changes in the water enthalpy may dominate the energy balance equation. The accurate

correlation used (Schmidt, 1969) provides thermodynamic consistency. However, the shape of the water phase envelope creates some problems. The Mollier diagram (Figure 7) shows regions where the enthalpy of the water can give multiple solutions. In some regions the vapour enthalpy does not change with pressure. The slope of the enthalpy function with respect to pressure is zero. As a result, the Newton-Raphson solution can converge without being correct and the movement of primary variables are not necessarily in the right directions. Other non-linearities in the correlations can also lead to multiple roots. To counter these problems, it is necessary to provide a better guess of the solution.

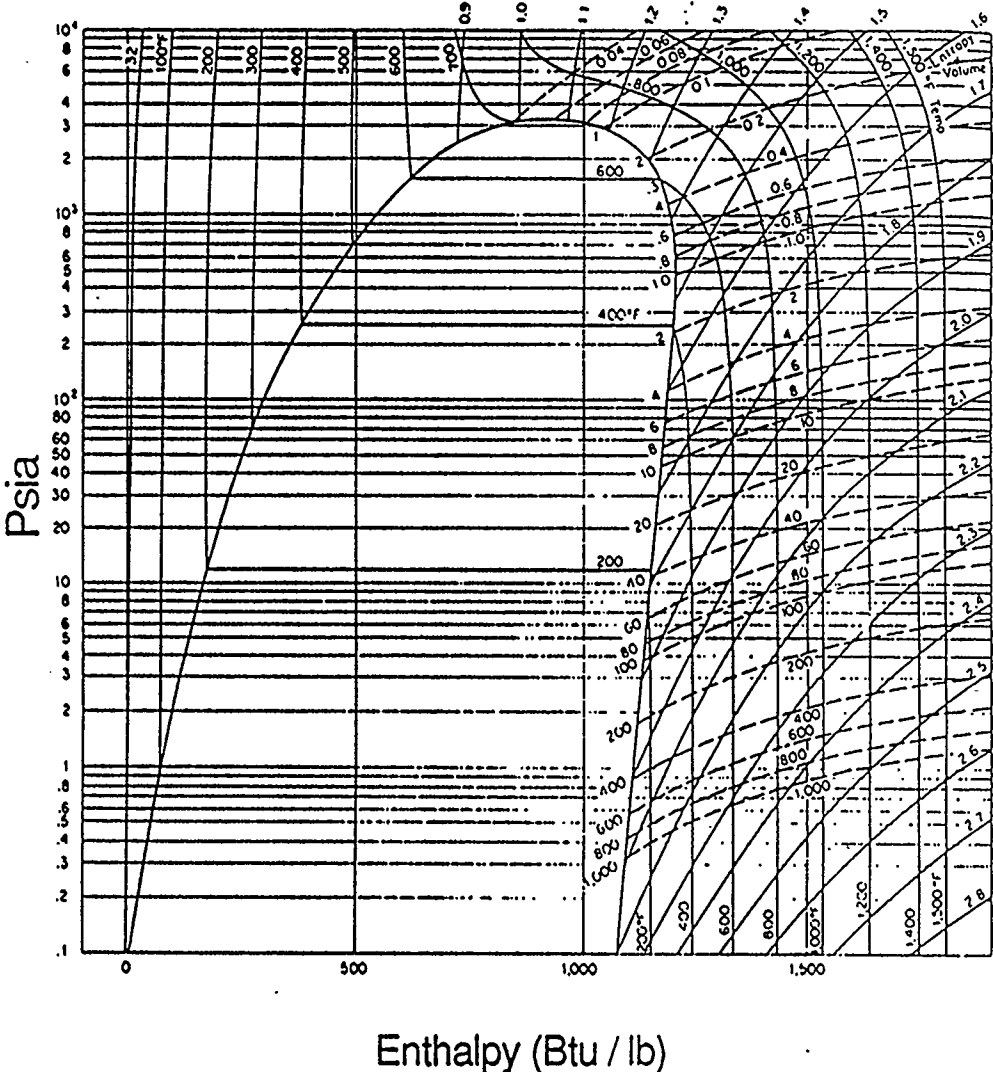
3.4 Fracturing Numerical Model Development

3.4.1 Relevant Information on Fractures in Unconsolidated Sands

3.4.1.1 Liquid Water Flow

An important factor in the numerical model development is the flow of the liquid water in the reservoir. In naturally fractured reservoirs the flow can be considered to be segregated (Settari 1979). In laminar flow with low capillary pressure in the fracture, phases separate due to density differences. In steam injection the flow in the fracture is not likely to be laminar, therefore the flow of liquid water is dispersed in the steam. Eventually, the water must settle to the bottom of the fracture, or it must find its way into the matrix. The path that the water takes is primarily a function of the relative permeability of water in the

Figure 7
Mollier Diagram
of Water



reservoir.

Some authors put the end point water saturation near 40 percent at higher temperatures (Bennion et al., 1985). Still others report that endpoints do not change with temperature (Farouq Ali et al., 1986). The endpoint for mobile water saturation is reported to be 6 percent for sand pack cores (Farouq Ali et al., 1986). The relative permeabilities of sand pack cores are probably close to those found in the thermally disrupted part of the reservoir. In an attempt to resolve this discrepancy in the relative permeabilities, information is inferred from field production data. If the endpoint mobile water saturation is very high, then the water will not be able to flow into the reservoir matrix, therefore it must stay in the fracture. On production, this water will then channel very rapidly to the well bore until all the water in the fracture is produced. Settari and Raisbeck (1981) showed that this is not the case. In general, clean water (no emulsions) production is observed throughout the first production cycle. Furthermore, the temperature profile of the production is nearly constant, which is not consistent with the water flowing back into the wellbore in a fracture. It is felt that the production of water can be better explained in terms of Darcy flow and the relative permeability of the fluids in the rock matrix. It is assumed that the condensed water finds its way into the reservoir matrix. Therefore, the water permeability endpoint must be much lower than reported by Bennion et al. (1985).

The flow of water into the matrix may be encouraged by the disruption of

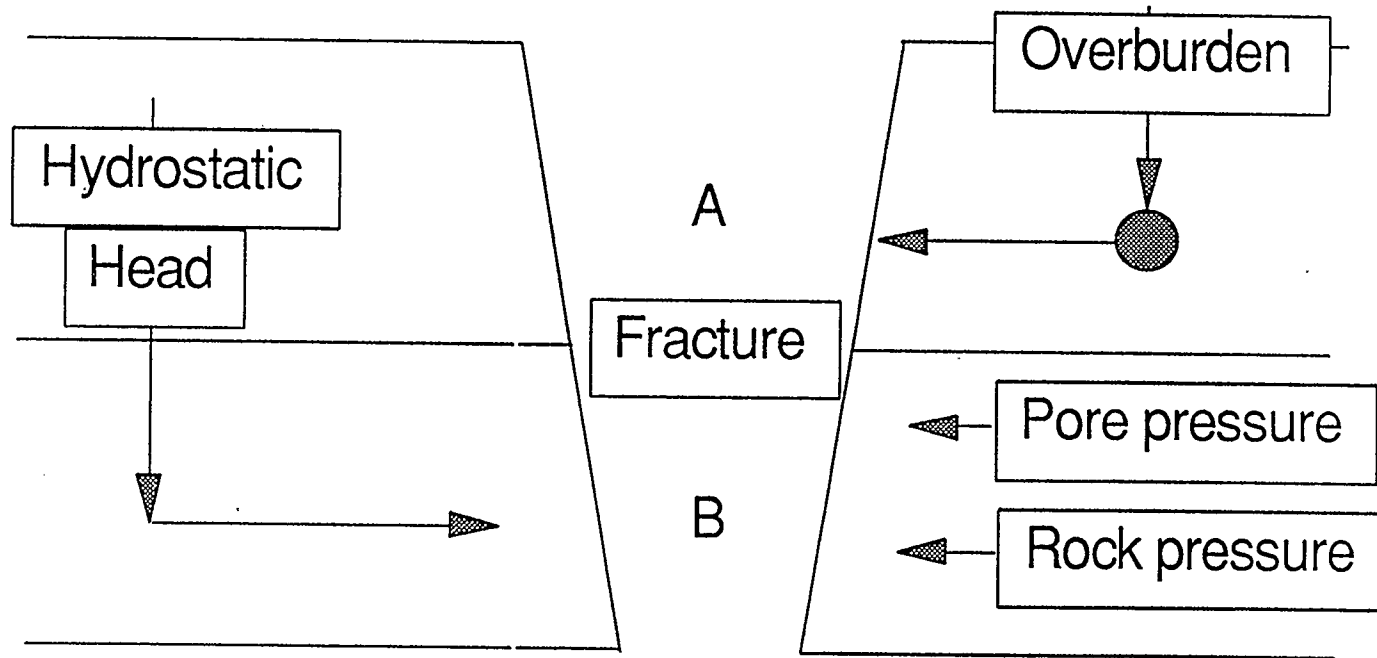
the matrix. Evidence for this possibility is the very low irreducible water saturation found in the packed cores. The condensing steam will likely form a film of water on the side of the fracture. This film, enriched with the water from the dispersed flow, will be forced into the matrix by the pressure difference between the fracture and the matrix (including capillary pressure).

3.4.1.2 Direction of Fracture Flow and Gravity Override

Usually vertical fractures form when the Poisson's ratio is small (an exception is made for very shallow reservoirs). Figure 8 shows a vertical fracture intersecting two grid blocks. The pressure in the fracture is nearly uniform, except for the relatively small hydrostatic head of the steam. However, the liquids in the matrix produce a large hydrostatic head. This means that the pore pressure in the bottom block must be higher than that of the top block. Furthermore, the rock stresses must also be higher in the bottom grid block. In order for this fracture to be stable, the fracture width must be greater at the top than at the bottom. The resistance to flow is therefore lower at the top. If the resistance is too high, not enough steam will flow in the grid block and hence the fracture will close. As a result, most formations will tend to fracture predominantly along the top of the reservoir.

In the case where the Poisson's ratio is small and the pore pressure is high, then the degree of override is affected largely by the capillary pressure in the matrix. Strong capillary forces can counteract the hydrostatic head and

The Forces Effecting Fracture Formation



Pressure at A = Pressure at B

Figure 8 Vertical Fracture through Two Grid Blocks

result in little preferential flow in the vertical direction. In those cases the fracture front is nearly vertical. The capillary pressure, however, is not a well known function in a disrupting thermal reservoir. Therefore, a degree of history matching will be required for the capillary pressure.

Another factor affecting the path of the fractures is the temperature. The higher the temperature the higher the Poisson's ratio. At the same time, the Young's modulus decreases with increasing temperature. The net result of these opposing factors is unknown. It is expected, however, that at shallower depths they tend to cancel out. In deeper reservoirs it is more likely that the Poisson's ratio dominates. Another factor due to temperature changes is the increase in the fracture roughness. The net result of the increase in temperature is to increase the resistance to fracture flow into hotter zones. Therefore the temperature effects tend to counter the main flow direction, namely the gravity override of the formation.

The anisotropic nature of the formation also influences the direction of the flow. The reservoir matrix is normally stratified, and the direction of flow is usually parallel to the bedding plane. Furthermore, the tectonic stresses favour the formation of fractures in a given direction. To model the anisotropic effects of the reservoir, a multiplication factor for the fracture permeability is used. This same multiplication factor is used for the matrix permeability, to prevent inconsistency problems.

3.4.2 Numerical Models Investigated

During the search for the optimum fracturing model, four fracture models were investigated. First was Ito's model. Ito's model was not pursued after finding the problems described in section 2.6.4. The remaining three models were developed in this work, in an attempt to capture the essence of the fracture concept described earlier.

The first model developed, consisted of dividing up the injection stream into a number of grid blocks, in an explicit fashion. The fraction of the total steam that is injected into a grid block is calculated from a complex equation. It is a function of the radial distance from the injection point, temperature and pressure of the matrix, direction from the injector and other factors. There are obvious problems with this model. However, a complete three cycle steam injection simulation was completed with this model yielding reasonable results.

The second model developed, is a hydrodynamic geo-mechanical approach to the problem. The fracture fluid flow is assumed to flow parallel to the Darcy flow in the matrix. In other words, the flow in the fracture can go in all directions. Since there is very little information about the fracture properties (i.e. Young's Modulus and Poisson's ratio), values are assumed. The permeability of the fracture is assumed to be high, but a reasonable number (based on the width of the fracture). The volume and area of the fractures per grid block are assumed to be small. Since at least one extra equation is required per grid block for every component in the fracture, plus the energy

balance, water is assumed to be the only component flowing in the fracture. If two phase flow is assumed, then three equations are required to describe the flow of water in the fracture, unless further assumptions are made about the nature of the flow. Settari and Raisbeck (1981) assume that the water and the steam flow at the same velocity in the fracture due to entrainment of water in the steam. Since this simplifies the problem, this is assumed here. An effective viscosity is assumed on the basis of how much of a given phase is in the fracture. The vapour fraction is determined from a iso-enthalpic flash, with provision for the formation of a single phase. There are some numerical problems with the model. The main reason that this model is not pursued is the total lack of any bases for some of the assumptions.

3.4.2.1 Fracturing Model Overview

The model finally settled upon is conceptually similar to the second model, however, the basis for the flow is different. In this case, the fracture flow is assumed to follow the path of the minimum rock opening pressure. Resistances to the fracture flow are upstream weighted. The effect of downstream resistances are accounted for in the fracture pressure gradient between grid blocks. Given a choice of direction, the steam will follow the path of the greatest potential (or requiring the least amount of work). Since there is a degree of uncertainty in the fracture pressure gradient and resistances a predictor-corrector method is developed to allow history matching of the flow.

Vertical fractures are assumed to form (backed up by evidence, see sections 2.6.2). The fractures are perceived to propagate in one direction at a time. With the changes in the matrix surrounding the fracture, the resistances increase. Finally the fracture changes course completely. The net result of the process is that the injected steam is distributed in all directions from the injector by the fractures. In a time averaged sense this is similar to Ito's conceptual model, although it is very different mechanistically (see Figure 3, top view).

Rather than describing the extent of the fracturing in terms of the unknown hydrodynamics, the fracturing extent is determined by enthalpy flow limited by heat conduction. The fracture grows until the heat conducted away from the fracture equals to the energy injected. Analytical models use conduction limited heat transfer to find the growing area of a steam fracture. In this case the heat conduction is used to find the heat absorbed by each grid block that the fracture intersects. The area per grid block is a history match parameter.

The area parameter is adjusted to fit observed dispersion in the reservoir. The temperature in the grid blocks near the injector is highly related to the heat transferred to them. With the temperature of the produced fluids known, an estimate of the heat transferred to the grid blocks near the injector can be estimated accurately. The thermal energy absorbed is proportional to the heat transfer area. This heat transfer area is adjusted until the temperature of the produced fluids matches that of the reservoir. The heat transfer area of

grid blocks deeper in the reservoir, is related to the heat transfer area of the grid blocks near the well by shape factors (i.e. grid block dimensions relative to the dimensions of the grid blocks near the well).

3.4.3 Numerical Model Development Constraints

Conceptually, Ito's model is at least partially correct, but improvements to the numerical model are necessary for the reasons given in section 2.6.4. Any numerical model proposed to replace Ito's model should optimize the following criteria:

1. **Simplicity.** The reservoir is complicated enough, without applying an overly complex model. There should not be a large number of adjustable parameters. Too many parameters lead to multiple solutions to the history match. The history match parameters should be constants whenever possible. If functions are used, then simplest forms possible are the most desirable. Furthermore, some aspect of production or injection should be fit by the adjustment of the parameter.
2. **Thermodynamic consistency.** A number of factors affect the thermodynamic consistency of the solution. The factor that is most controllable during fracturing is to associate heat flow with an appropriate amount of mass flow. This will increase the probability of the existence of a solution.
3. **The model must be reasonably mechanistic.**
4. **The incremental cost in terms of computer time should not be too large.**

Therefore the addition of equations to the system must be kept to a minimum, along with the calculation of the fracture properties.

3.4.4 Numerical Model Concept

To define the fracture flow in the unconsolidated sands, it is necessary to know the fracture pressure gradient, leakoff rate into the matrix, and the resistances to the flow. Technically this problem is insolvable. There are too many unknowns and too few knowns. It is possible, however, to get a good estimate of the process. This is done by concentrating on what is known (i.e. injection rates and matrix pressure) and applying two adjustable (history match) parameters. The first history match parameter is a dispersion coefficient, which gives an indication of how far the fractures penetrate into the reservoir. The second is a tuning parameter for the gravity override of the fractures.

It is necessary to know the resistances and the fracture pressure gradient in the fractures to divide up the flow into the various downstream directions. To quantify the resistances and the pressure gradients in the fracture is difficult, if not impossible. However, it is possible to infer information about these quantities from other sources, namely the pore pressure of the matrix.

Conceptually, the injected steam flows into the grid block's fractures where some of the fluids are absorbed. The unabsorbed fracture fluids are passed onto the adjacent grid blocks (Figure 9). The leakoff (absorbed fracture

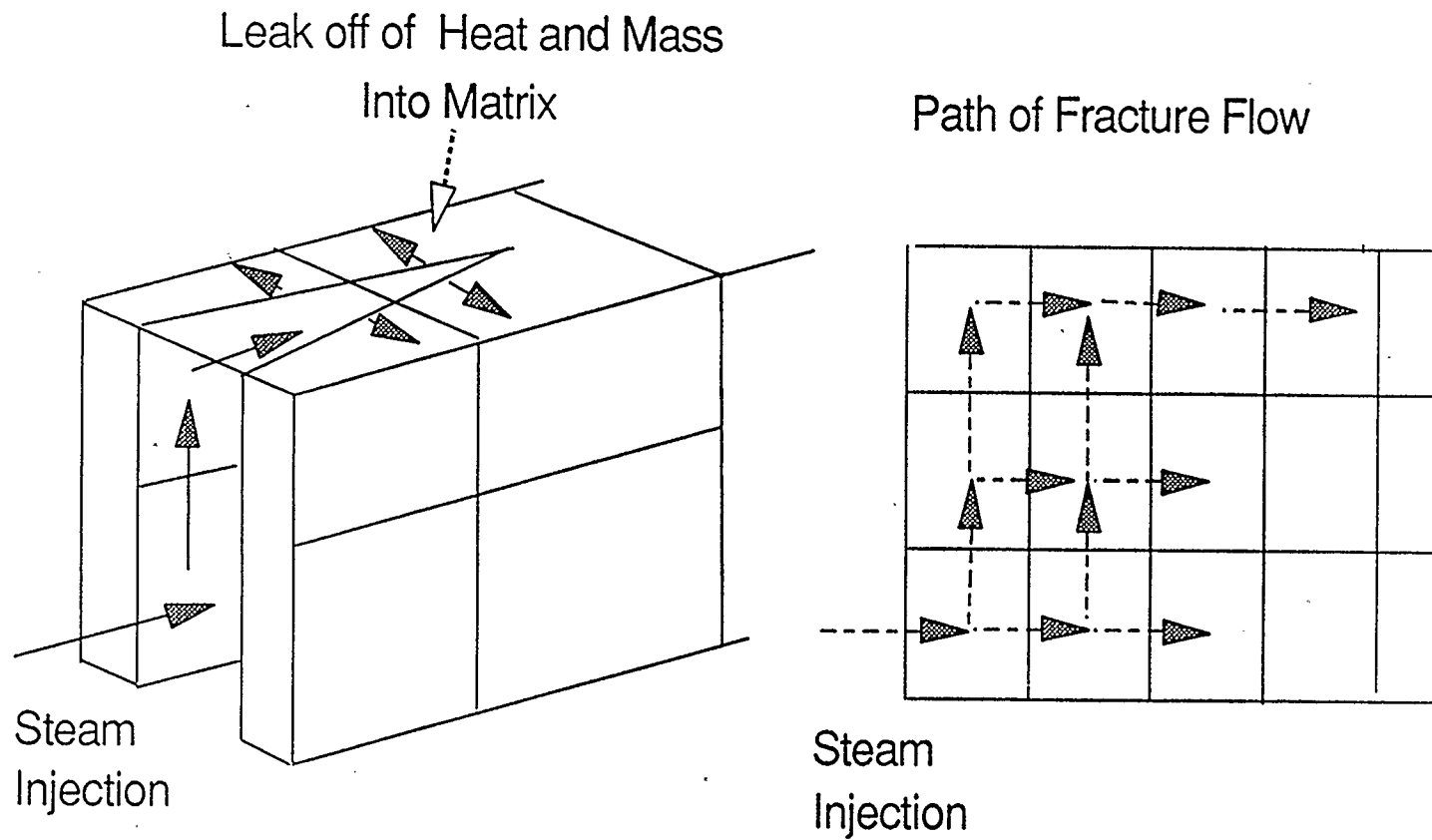


Figure 9 Numerical Model Concept

fluids) is assumed to be controlled by conduction. Given the flow into the grid block's fracture, the flow out in the fractures is known.

3.4.5 Assumptions

If the assumptions are plausible, then the result from the model is expected to be a reasonable. A discussion of the necessary assumptions follow.

1. The Fracture Makes Its Own Permeability

The fracture does make its permeability with geo-mechanical fracturing. As the injection rate is increased the fracture pressure increases, thus the width of the fracture increases. Settari and Raisbeck (1981) assume that the pressure drop under this type of fracturing is negligible. However, there are resistances in the fractures. These resistances are important in determining the direction of fracture flow in the reservoir.

In thermal unconsolidated reservoirs, the degree of uncertainty in the actual resistance is large. However, to divide up the flow into the downstream directions it is only necessary to know the ratio of the resistances in each direction. An analogy of this is the division of an electrical current into two conduits. The ratio of the current, I , flowing in each direction is

$$\frac{l_1}{l_2} = \frac{V_1 R_2}{V_2 R_1} \quad 3.2$$

where V is the voltage and R is the resistance to the flow.

As in this case, the resistances are generally upstream weighted. The permeability (and the viscosity) at the interface between any two grid blocks is calculated from the state variable of the upstream grid block. Upstream weighting means that the permeabilities in all downstream directions are the same. The only factor which makes a difference to the resistance is the shape of the grid block (aspect ratio). Therefore, the resistances with upstream weighted permeabilities are proportional. Essentially upstream weighting lumps all the fracture path determination factors into the fracture pressure gradient and the shape factors.

For the purposes of the simulator, it is only necessary to give an arbitrary constant fracture permeability to divide up the flow. Implementation of this requires the permeability to rise rapidly to a high value with pressure. The reason that this value is a function of pressure is to smooth the fracture development.

In fractured flow, however, the downstream resistances cannot be completely ignored. The downstream resistances are a major force in determining the path of the fractures. To compensate for these resistances the fracture pressure gradient is modified. The form of the modification or correction is dependent upon the direction in which the resistances drive the

fractures.

Although the resistance are unknown, they can be considered to be a function of pressure and temperature. On a local scale, all of the fracture resistances can be linearized about an upstream point, $f(T_o, P_o)$,

$$R = \left(\frac{\delta f}{\delta P} \right)_T (P - P_o) + \left(\frac{\delta f}{\delta T} \right)_P (T - T_o) + f(T_o, P_o) \quad 3.3$$

where T and P are the temperature and pressure of the downstream grid block respectively. The pressure deviation's proportionality constant (Young's modulus) is small. In most cases the change in resistance due to pressure will be small. This is further reinforced by the low matrix pressure gradients found in the fractured zone. The deviation in the resistance due to the temperature is difficult to quantify and to separate from other factors. As the temperature rises the roughness of the wall of the fracture increases, increasing the resistance. Higher temperatures result in an increase in the Poisson's ratio which also increases the resistance. At the same time the Young's modulus increases, decreasing the resistance to the flow.

There is another resistance to be considered outside of the realm of Equation 3.3. This is the resistance due to the energy required to propagate the fracture tip. In the region where the fracture tip is propagating, the fracture pressure drop is large. The fracture pressure falls from the injection pressure (or close to it) to a pressure equal to the pore pressure (Settari and Raisbeck, 1981). The large resistances in the tip region may be the dominant factor in

the determination of the fracture path. This is especially true if the fracture path is continuously changing. The amount of energy which is dissipated in the fracture tip is a function of the rock opening pressure (pore pressure plus the horizontal stress, Equation 2.5). Low rock opening pressures require less energy to propagate the tip. Therefore, the fracture will follow the path with the lowest rock opening pressure.

In order for the history match to be successful, there cannot be too many adjustable parameters. Therefore, it is best to lump temperature dependent resistances into one adjustable parameter. The net impact of not including the temperature effects, is the gravity override of the formation by the fractures is excessive. The correction parameter must act in the opposite direction. The temperature dependent fracture pressure is shown later.

2. Only Gas Flows in Fractures.

Often during steam injection pilots the quality of steam is less than one hundred percent. It is believed that initially the fractures that form are of the type described by Settari and Raisbeck (1981). These wide, open space fractures allow the steam to carry the injected and condensed water through the reservoir via entrainment. In this way the liquid water is dispersed through the reservoir. To accommodate the entrained flow is a simple extension to the model being developed here.

As the temperature rises in the fracture, it is conceptualized that the

fracture width is restricted. Sand falling into the fracture, changes in the path and roughness of the wall will knock out any liquids flowing in the vapour stream. Under these circumstances, liquid water will not flow in the same fracture or at least the same part of the fracture because of density and viscosity differences between phases. If the matrix cannot accommodate the water flow, then it is better to simulate it through transmissibility multipliers. This does not cause any numerical problems because the water is in the liquid state. In any case the maximum error in the thermal energy distribution in the reservoir is usually less than ten percent due to this assumption. The error ($Error_{max}$) can be calculated from

$$Error_{max} = \frac{(1-X)H_{sl}}{(H_{sv}X + H_{sl}(1-X))} \quad 3.4$$

where X is the steam quality and H_{sv} and H_{sl} are the enthalpy of the saturated vapour and liquid respectively. This error becomes large in two cases. Firstly, when the steam quality is low. Secondly, when the steam is near the critical point (see Figure 7). Usually these situations are avoided since the cost of heating the reservoir increases as both situations are approached.

3. The Fractures have no Volume

On a reservoir scale the fracture volume is very small relative to the matrix and can be assumed to be zero. With no volume, there can be no

accumulation of material in the fracture. This lack of accumulation results in instantaneous dynamics, which improves the overall efficiency of the numerical procedure. Convergence to the solution is faster and as shown later, the number of required equations is minimized.

4. Fracture Temperature is Saturated Steam Temperature

Temperature can be calculated from the pressure by using the vapour pressure curve. This assumes that the steam in the fracture is saturated.

T_{fracture} equals $T_{\text{saturated}}$ at the partial pressure of the steam.

5. Heat Transferred to the Matrix is Heat Conduction Limited

The heat transferred from the fracture to the matrix within a grid block (volume, V), assuming the latent heat is conducted into the matrix, is given by

$$Q = A_d k_c V (T_{\text{fracture}} - T_{\text{matrix}}) \quad 3.5$$

Where Q is the heat transferred, k_c is the thermal conductivity of the matrix and " A_d " is the area of the fracture per cubic metre per gradient length. " A_d " is a history match parameter which describes the interaction between the matrix and the fracture. Clearly the fracture steam does not come into thermodynamic equilibrium with the grid block that it is flowing through, therefore some of the steam bypasses the grid block. This bypassing steam generates dispersion of the thermal energy through the reservoir. " A_d " is determined by the history matching of the production temperature of the reservoir. Large values of " A_d "

indicate Darcy flow. Smaller values indicate dispersion in the reservoir. Since " A_d " is a relative term, it can be used to compensate for errors in the equation. These errors may be due to the assumption 5 or in the temperature difference between the fracture and the matrix.

6. The Fracture Pressure Gradient can be Estimated from the Rock Opening (Closing) Pressure

In view of the uncertainties in the system, there are a number of possible ways of estimating the fracture's pressure. One possibility is to use the rock opening pressure. The objective of the estimate is not to provide absolute pressures, but rather relative fracture pressure gradients. The error in the fracture pressure gradient should lead to excessive gravity override. Then temperature dependent factors, which act against the general flow, can be used to compensate for this error (along with the temperature dependent factors). However, the initial estimate should be as accurate as possible so that the correction factor is small. Accurate estimates give more meaning to the temperature dependent term.

It is not necessary to know the absolute pressures to divide up the flow out of a grid block. Only relative values are necessary. The use of relative values has a further advantage of minimizing the error in fracture pressure gradient, due to the estimate of the fracture pressure. Furthermore, the implicitness of the solution has a self correcting character.

At greater depths the change in the Young's modulus is not likely to cancel the increase of the Poisson's ratio due to the temperature rise. More of the net overburden pressure is transmitted to the fracture. Without a corresponding decrease in the Young's modulus, the width and the fracture permeability must both decrease. This increase in the resistance in the hotter zones has an effect on the gravity override of the formation. Furthermore the increased overburden pressure will increase the rock opening pressure. The fracture tip is less likely to be propagated in the direction of high rock opening pressure, because of the increase in the amount of the work which must be done.

The correction to the fracture path must act in the opposite direction to the forces generating gravity override. A modified version of the rock opening pressure provides the necessary form

$$P_{fracture} = P_{pore} + (\sigma_v - P_{pore} + \rho_{rock} \Delta z g) * v(T) \quad 3.6$$

where $v(T)$ is a pseudo Poisson's ratio as a function of temperature. The overburden pressure, σ_v , can be estimated with well known equations. The rock density, ρ_{rock} , can also be found from the literature. The function $v(T)$ is adjustable and one possible form is

$$v(T) = v_0 + v_T (T - T_{initial}) \quad 3.7$$

where the variable v_T is a history match parameter with an order of magnitude

of 0.001 and v_o is the initial pseudo Poisson's ratio. The error in the fracture pressure gradient can be compensated with this form. The temperature correction for the change in the Poisson's ratio acts against gravity override of the formation. The error in the fracture pressure gradient leads to excessive gravity override. Therefore, a small addition to the temperature correction can account for the error.

Near the propagation of the fracture tip, the fracture pressure form (Equation 3.6) will provide good estimates of the fracture flow direction. Tip propagation may be the dominant force in the determination of the direction of flow in the whole reservoir. If this is the case, then there will be little error in using Equation 3.6 to calculate the relative fracture pressure gradients.

The use of Equation 3.6 for calculating the fracture pressure gradient in the established part of the fracture is complicated by the missing net fracture pressure term. This term is the pressure required to compress the rock, which gives the fracture width. To a degree this will cancel out with the net fracture pressure of the upstream grid block when calculating the fracture pressure gradient. The error is further diminished by the calculation of the flow ratio (analogous to Equation 3.2). The slight excessive fracture pressure gradient in the vertical direction can be considered to be compensation for the lower resistances in that direction. Both the lower pore pressure and the lower rock stresses will lead to smaller resistances in the vertical direction.

In shallow reservoirs the pore pressure dominates the fracture pressure.

Small increases in the pore pressure will result in it reaching the overburden stress. Therefore, the impact of the rock on the fracture path is minimal. Furthermore, changes in the Poisson's ratio are likely to be cancelled by the change in the Young's modulus. The rock stresses can be completely ignored. However, if desired, the extra pressure on the fracture due to the rock density can be added on to the matrix pressure gradient to give the fracture pressure gradient. The correction for temperature dependency of the roughness of the walls, is best done with the temperature dependent capillary pressure. Matching the capillary pressure and the temperature factor will ease the history match.

The form of Equation 3.6 has a number of advantages. First of all it is simple. This makes the history matching of the temperature effects easier. Secondly, the form of the equation keeps effects of the pore pressure and the rock stresses in the proper proportions. As the pore pressure increases, the impact of the changes in the Poisson's ratio is diminished. It is also applicable in various regions of the fracture. Thirdly, history matching may be aided by inferring information from the injection pressure or the injectivity. The equation form is not intended to match the injection pressure. Its only purpose is to provide relative fracture pressure gradients for the division of flow. However, if the error in the fracture pressure gradient is small, then information about the nature of reservoir can be determined.

There is also a number of disadvantages with Equation 3.6. Firstly,

there may not be enough adjustability to compensate for large changes in the resistance. Secondly, the dynamics is not accounted for. Rapid growth could have an effect on the solution. Thirdly, the gradients (temperature, pressure, etc.) within the grid block matrix are not accounted for. Inherently the model assumes that the matrix is homogeneous and has no gradients. Clearly, this is not the case. These gradients probably will have some effects on the path the fractures will take in the reservoir.

An estimate of the actual pressure in the fracture is required to calculate the fracture fluid properties. This estimate does not have to be very accurate to give good values for the properties. Large changes in the pressure only result in small changes in the vapour enthalpy and temperature (Figure 7). In view of the insensitivity, one good estimate is to assume no pressure drop in the fractures, and that the fracture pressure is the same as the injection pressure.

3.4.6 Implementation

All the conservation equations in the balance equations have the fracture flow terms added to them. These modified conservation equations, about a grid block, have the form:

$$\begin{aligned} (IN - OUT + GENERATION - ACCUMULATION)_{matrix} \\ +(IN - OUT)_{fracture} = 0.0 \end{aligned} \quad 3.8$$

which is in keeping with the previous assumptions. The $IN_{fracture}$ term has

three elements. The first element is the injection terms to the grid block in the gas phase. The next element is any matrix gas that finds its way into the fracture. The last element is the fracture flow out of any adjacent grid block, into the grid block.

Given the above assumptions, the fracture equation and the matrix equations are functions of the same state variables. With no additional degrees of freedom, there is no need for more equations to be added to the Newton-Raphson set. The two equation sets can be added together. This keeps the time requirement of the equation solver to a minimum. Only a single equation is required to describe the flow of a component or energy in the fractures and the matrix.

The matrix energy balance equation in one dimension, in finite-difference form is

$$\begin{aligned} \frac{V}{\Delta t} \delta \left[\phi \sum_{j=1}^{N_p} \rho_j S_j U_j + (1-\phi) M \chi (T-T_I) \right] = \\ \sum_{j=1}^3 \Delta \left[\tau \rho_j \frac{k_{rj}}{\mu_j} H_j (\Delta P_m + \Delta P_{cj} - \gamma_j \Delta z) \right] + \Delta(\tau_c \Delta T) + \Delta(\tau_r \Delta T^4) \\ + \sum_{n=1}^{N_{rea}} H_{rea} - Q_{ip} + A_d k_c (T_f - T) V \left(1.0 + \frac{1.0}{\lambda_f} H_{Lf} \right) \end{aligned} \quad 3.9$$

where the last term is the energy transferred from the fracture to the matrix.

The left hand side of the equation is the accumulation of energy in the grid block. The first term on the right hand side is the flow of energy through the

matrix due to convection. The second and third terms are the energy transferred by conduction and radiation in the matrix. Q_{ip} is the heat injected or produced from the grid block matrix (not the fractures). P_{cj} is the capillary pressure of the phase, however it is zero for phases other than liquid water.

The fracture energy balance in one dimension in finite-difference form is

$$0.0 = \Delta \left[\tau_f \frac{\rho_f}{\mu_f} F_E H_f (\Delta P_m + \Delta P_R - \gamma_f \Delta Z) \right] - A_d K_c (T_f - T) V \left(1.0 - \frac{1.0}{\lambda_f} H_{Lf} \right) \quad 3.10$$

where the left hand side of the equation is the accumulation (zero) and F_E is the fraction of the enthalpy flowing in which flows out of the grid block's fractures. F_E is calculated at every time step and is defined by the fraction

$$F_E = \frac{\sum \text{Enthalpy Flowing Out}}{\sum \text{Enthalpy Flowing In}} \quad 3.11$$

The mass balance equation(s) in finite-difference form is as follows

$$\frac{V}{\Delta t} \delta \phi \sum_{j=1}^{N_p} \rho_j S_j x_{ij} = \sum_{j=1}^{N_p} \Delta \tau_{pj} \rho_j x_{ij} \frac{k_{ri}}{\mu_j} (\Delta P_m + \Delta P_c - \gamma_j \Delta Z) + \sum_{n=1}^{N_{rea}} q_{rea} - q_{ip} + \Delta \left[\tau_f \frac{\rho_f}{\mu_f} F_E x_{if} (\Delta P_m - \gamma_f \Delta Z + \Delta P_R) \right] \quad 3.12$$

where P_R are the rock stresses. The rock stresses are a function of the matrix state variables. The mass transfer terms between the fracture and the matrix

cancel when the two equations are added together. Only the difference between the "flow in" and the "flow out" term of the fracture equation remains. The source and sink terms, q_{ip} , do not include the injected gas. This term is added to the "in" term of the fracture mass balance portion of the equation.

3.4.6.1 Mass and Heat Exchange Between Matrix and Fracture

The amount of latent heat conducted from the fracture to the matrix is assumed to be the limiting factor for heat and mass transfer. The removal of latent heat results in the formation of liquid water. This condensate is assumed to flow into the matrix. The condensate flow carries heat into the matrix by convection. Therefore, the total heat flowing into the matrix from the fracture is the heat in the condensate plus the heat brought in by conduction. The mass flow rate into the reservoir matrix is the condensate rate. Although the above discussion is for water, other gaseous components in the fracture are dealt with in a similar way.

Incorporating the flow of gas from the matrix to the fracture is not as easy. Elaborate mechanisms can be thought of to describe this interaction, however in view of the uncertainties the model must be kept simple. Therefore, a low percentage of the mobile gas phase flowing from one grid block to another in the matrix is assumed to find its way into the fracture. This parameter will be difficult to history match, however, it is not very important to the fit.

3.4.6.2 Division of Enthalpy and Mass Flow in Downstream Fractures

The amount of energy absorbed by the grid block is given by Equation 3.5. The enthalpy flowing out of the grid block in the fractures is given by the difference between the enthalpy flow in and the amount absorbed. The enthalpy available to the downstream blocks is

$$H_{out} = \sum H_{in} - H_{absorbed} \quad 3.13$$

This enthalpy flows onto the downstream blocks. To divide up the enthalpy into the downstream blocks, a number of steps are followed. First the maximum possible fracture flow is calculated in each downstream direction:

$$\text{Maximum Flow} = \frac{K_f \rho_s \Delta P}{\mu_s \Delta x} \quad 3.14$$

K_f is the fracture conductivity assumed. Secondly, the sum of these maximum flow values is then found. Usually only a very small fraction of this sum is available to the downstream blocks (because of the very high assumed conductivity of the fracture). The available enthalpy is then divided up proportionally to each direction's maximum possible flow. In practice the factor F_E of Equation 3.11 is modified to the multidimensional case, by the multiplication of the fraction of the sum. Thirdly, the available mass associated with the enthalpy is divided up into the downstream blocks on the same basis as the enthalpy. Once the available vapour enthalpy is zero or less the fracture propagation is terminated.

3.4.6.3 Simulator's Matrix Disruption

With disruption, the matrix porosity and permeability increase permanently. Ito (1984) assumes that this is a function of pressure. In view of Butler's work (1986), perhaps it is better to describe this in terms of temperature. In any case this process is far too complicated to describe on the basis of microscopic mechanisms, and must be described on a macroscopic basis. For this work hysteresis in the porosity and the permeability are assumed to be a linear function of temperature. The historically high values of the permeability or the porosity are the values used at later times. History matching these parameters is dependent upon how well the surface heave can be measured.

3.4.7 Model Evaluation

The model does a number of things quite well. Firstly, it allows for a larger time step. The dynamics in the matrix is slower than with Darcy flow, therefore larger time steps can be taken. Secondly, the gravity override profiles are realistic. Finally, the model allows for an easily history matched dispersion parameter. This gives a measure of how deep into the reservoir the heat is penetrating. It is surprisingly independent of change in other input parameters.

On the other hand, the model has some weak points. Mass transfer to the matrix is assumed to be associated with heat transfer. While steam is flowing in the fracture, this is a good assumption. If the steam leaks off into the

matrix, then it would not be possible to maintain the fracture and the flow would revert to Darcy flow. History matching of " A_d " accounts for some leak off of steam. However, when only hydrocarbon gas is left in the fracture, mass transfer limits the flow. Without further assumptions, it is not possible to simulate this effect with this model. Furthermore, if water is flowing in a separate fracture channel (not dispersed flow), it cannot be simulated with this model.

3.4.8 History Matching Fracture Parameters

The first cycle temperature of produced fluids is a low sloped (Ito, 1984) nearly linear function. This allows for the history matching of the dispersion coefficient " A_d ". Matching this parameter is very easy, since it has the strongest effect on the temperature of the grid blocks. A high degree of confidence can be given to the degree of the dispersion in the reservoir. This parameter is independent of the other variables in the simulator.

The distribution of the heat in the reservoir cannot be done with the same degree of confidence. The capillary pressure, rock stresses and temperature dependent resistances all affect where the fractures go in the reservoir. The complexities could lead to multiple fits to the gravity override. Nearly the same gravity override of the reservoir can be achieved in a number of different ways. The problem is to get enough information from the field and from the laboratory to get an unique fit to the production data. If steam

breakthrough is observed on the first cycle then the parameters affecting the override can be fit. Usually this will not be the case. Without breakthrough, the actual distribution of the fractures is not known. Some information may be derived from the temperature of the production. If the capillary pressure is low in the matrix, then density differences lead to convection cells, which result in higher temperatures in the upper grid blocks. Depending on the degree of gravity override, the slope of the production temperature will be slightly affected. More information can be deduced from the changes in injected pressure and/or changes in the injectivity.

The hydrostatic head alone can create a very strong gravity override. In shallow, thin reservoirs it would seem reasonable to ignore the rock stresses. Usually, the lack of information on the capillary pressure will mean that it will have to be history matched. It is difficult to match the capillary pressure separately from other variables. Therefore, it may be better to history match a pseudo capillary pressure which encompasses these other variables. This pseudo capillary pressure could be used to fine tune the gravity override of the formation.

In deeper reservoirs the rock stresses becomes more important. Changes in the Poisson's ratio will have a large effect on the gravity override of the formation. It is then necessary to correct the fracture pressure with Equation 3.6. The initial pseudo Poisson's ratio, v_o , of Equation 3.7, can be found from the initial fracture pressure. However, the temperature dependent

component, v_T , of Equation 3.7 is not easily found. Only scant convoluted information is available to fit to this component. However, there is only one global parameter to fit. With some knowledge of the capillary pressure, this parameter can be estimated with a reasonable degree of accuracy.

3.4.11 The Second and Subsequent Injection Cycles

On the second cycle, the matrix near the well bore is partially drained of its fluids and is disrupted. The higher rock stresses (due higher Poisson's ratio) requires more fracture pressure to allow the same flow rate of the steam. This results in the higher injection pressures observed on the second cycle.

Furthermore, near the well bore the (drained and disrupted) matrix is very permeable to the flow of gas (i.e. steam). It is likely that steam flows through this region in channels (or by Darcy flow), without fracturing the matrix.

Fracturing is believed to occur only when steam contacts cooler parts of the reservoir. The flow through matrix near the well bore may also contribute to the higher injection pressure observed.

This work concentrates on the first cycle.

Chapter 4

Simulation

The base case for the simulation is a two dimensional 40 grid block system. The length (horizontal direction) of 80 meters is equally divided between 10 grid blocks. The vertical direction is divided up into 4 grid blocks. The bottom two are 2 meters in height and the top two are 1.5 meters in height. The width of the reservoir is 8 meters. Injection occurs on the bottom grid block on one of the sides. A producer is always on the other side of reservoir from the injector. However, the main production is when the flow direction is reversed and the production is allowed back through the original injector (cyclic steam injection).

The viscosity of the Athabasca bitumen is calculated from Mehrotra's (1992) equation

$$\log(\mu + 0.8) = \sum \psi_i 10^{b_1} T^{-b_2} + \sum \sum \psi_i \psi_j B_{ij} \quad 4.1$$

where ψ represents the geometric mean of mass and mole fraction of the component, b_1 and b_2 have values of -0.89 and -0.0593 for the gas and 9.817 and -3.667 for the Athabasca bitumen respectively and B_{ij} is a binary viscous interaction term defined by the equation:

$$B_{ij} = A_0 + A_1 T \quad 4.2$$

where the parameter A_0 and A_1 have values of -2.071 and 0.0185 respectively and T is in Kelvin. In cases where the bitumen is not saturated, it is assumed that the equation will hold for different mole fractions of gas dissolved in the bitumen. Since information on the whole range of gases dissolved in the bitumen is not available, the gases dissolved in the oil are assumed to be characterised by ethane (the parameters used reflect this assumption).

The viscosity of steam, μ_s (mPa's), (Butler, 1991) is shown below:

$$\mu_s = (-0.001 + 0.0029 \ln(P_s + 100)) \quad 4.3$$

where P_s is the partial pressure of the steam in psia. The mixing rule employed for the gas phase is from Reid et al. (1977), and is as follows:

$$\mu_g = \frac{\sum_{k=1}^{N_{cg}} X_k \mu_k (M_{kw})^{0.5}}{\sum_{k=1}^{N_{cg}} X_k (M_{kw})^{0.5}} \quad 4.4$$

where X_k is the mole fraction of component k in the gas, M_{wk} is the molecular weight of component k , N_{cg} is the number of component in the gas phase and μ_k is the viscosity of the pure gas.

Density of the bitumen is calculated from an equation fitted to the data from Mehrotra and Svrcek (1985). The characteristic gas is assumed to be ethane. Ethane is the closest hydrocarbon gas in molecular weight to the gas

produced by the cracking reactions (Belgrave et al.,1990). For the purposes of the density calculation, the bitumen is assumed to be saturated at all times at the partial pressure of the gas. The density of the bitumen, ρ_b , (kg/m³) is

$$\rho_b = ((-1.46 E-8 P_g + 1.0035) + 3.14 E-5) (1.0 - 10^{-9} (P_T - P_g)) \quad 4.5$$

where P_g is the partial pressure (Pa) of the gas, T is the temperature in degrees Celsius, and P_T is the total pressure (Pa).

The density of the liquid water is calculated from the accurate water correlation (Schmidt, 1969), for which the computer listing is provided in Appendix E. The density of the gas phase is calculated from the SRK equation of state.

The K values for the gas, bitumen and water are calculated using Raoult's law or Henry's law. Henry's law is used to calculate the K values for the gas component (see Appendix B). The original data for the hydrocarbon gas K values is from Xu and Hepler (1990). The vapour pressure of water is calculated from the water correlation (Schmidt, 1969). The K value for the bitumen (maltenes) is calculated as in Appendix B. The water and the gas component's K values are linearised about the previous time step. The gas component's exponential factor, *efac*, (as defined in Appendix C) is equal to 1.5 and the initial carbon number, *CNI*, is equal to 1.5, for all of the runs. Enthalpy of the water and steam are calculated from the water correlation (see Appendix E) (Schmidt, 1969). Enthalpy of the gas component is calculated

from ideal gas enthalpy (Reid et. al., 1977). The gas in the liquid oil phase is assumed to have a fixed heat of solution given by Xu and Hepler (1990). The bitumen enthalpy, H_b , (kJ/kg) is calculated from a heat capacity equation (Butler, 1991) and is as follows:

$$H_b = (0.349 T + 3.668E-4 T^2 - 2.135E-6 T^3) 2324.6 \quad 4.6$$

where T is in °F (note that there is an unit conversion factor in the equation). The latent heat of the bitumen, an assumed fixed value of 50E6 J/kmole, is added to the liquid enthalpy to give the vapour enthalpy. Little error is introduced by the fixed value of latent heat, since the mole fraction of bitumen in in the gas phase is very low.

The initial porosity is 35 percent. The maximum permanent increase in porosity due to the matrix disruption is assumed to be 2 percent. Porosity is increased with increasing matrix temperature. Disruption is assumed to start at 30 °C and reach a maximum at 150 °C. Permeability does not vary for these runs and is set at 1 Darcy (μm^2).

The injection rate is an important consideration in testing the fracturing model. The injection rate must be high enough to ensure that the matrix fractures. Furthermore, the model must be able to handle commercially used injection rates. The size of the model reservoir has to be taken into account when deciding the injection rate. Since the chosen model size for this test is

small, the injection rate must be adjusted accordingly. The full pattern injection rate used is 11 cubic meters of steam cold water equivalent per day. This injection rate is three times the value reported by Forsyth et al. (1981) per grid block volume for a commercial operation. The model can easily handle this rate. The injection pressure (above the fracture pressure) is 650 psia (4.5 Mpa) and injection is at a constant rate. The steam is slightly superheated at a temperature of 250 °C. Injection and production cycles are 50 days long. Production occurs against a back pressure of 250 psi (1.7 MPa) and a productivity index of 0.2.

The initial pore pressure is 300 psi (2 Mpa). The bitumen saturation is 80 percent with no initial gas saturation and 77 percent when initial gas is present. The initial water saturation is 20 percent. The mole fraction of gas in the oil is 20 percent of the saturated value if no initial gas phase exists. Otherwise, it is saturated. The initial temperature is assumed to be 11 °C. The overburden heat losses are assumed to be zero.

Except for the sensitivity studies, the heat transfer area coefficient, " A_d ", is 0.5 meters⁻². The thermal conductivity of the rock matrix, k_c , (J/m°C) is as follows

$$k_c = (1.04 - 1.30\phi + 0.77(1.0 - S_o)) * 1.73 \quad 4.7$$

where ϕ is the matrix porosity and S_o is oil saturation. The rock heat capacity, M_f , (kJ/kg°C) is given by:

$$M_f = (0.170 + 2.11E-4 T - 1.494E-7 T^2) 4184 \quad 4.8$$

where T is in $^{\circ}\text{F}$ (note that there is a unit conversion factor in the equation).

The initial pseudo Poisson's ratio is assumed to be 0.2 (Settari and Raisbeck, 1981). The temperature correction value is assumed to be 0.001. The density of the rock is assumed to be 2000 kg/m^3 and the overburden stress is assumed to be 3.0 Mpa. The anisotropic factor is 1.5 times in the horizontal direction.

The water capillary pressure and the relative permeabilities are a problem. The interfacial tension decreases linearly with temperature (Farouq Ali et al., 1986). However, from the same paper the endpoints of the relative permeability curve do not change with temperature. If the interfacial tension changes, it would be expected that the residual saturation would change. In fact others report the relative permeabilities do change with temperature (Bennion et al., 1985), however in the opposite direction than what would be expected with a decrease in interfacial tension. To add to the confusion, the residual oil saturation reported in the lab is about 50 percent, whereas field reports give 70 percent oil recovery from Athabasca pilots (Redford, 1986). In the absence of any production data in the literature for Athabasca bitumen, it is not possible to history match the relative permeabilities. Therefore, the relative permeabilities used in the simulations are arbitrary. However, the relative permeability curves have been adjusted to give what is thought to be a reasonable production profile. These curves are shown in Table 4.1.

Table 4.1 Relative Permeability Curves (Stone's Second Model)

S_w	k_{rw}	k_{row}	1.0-Sg		
			sl	k_{rg}	k_{rog}
0.135	0.000	1.000	0.00	1.00	0.00
0.15	0.001	0.900	0.10	0.90	0.10
0.20	0.003	0.800	0.20	0.50	0.20
0.21	0.005	0.790	0.30	0.40	0.40
0.25	0.030	0.700	0.50	0.30	0.50
0.30	0.070	0.600	0.60	0.25	0.60
0.40	0.130	0.500	0.80	0.10	0.70
0.50	0.190	0.400	0.90	0.04	0.80
0.60	0.250	0.300	0.95	0.001	0.90
0.70	0.400	0.015	0.96	0.00	0.94
0.75	1.000	0.000	1.00	0.00	1.00

The capillary pressure is normally a function of saturation. In the thermal reservoir, it is also a function of the degree of disruption of the matrix and temperature. Therefore, the capillary pressure has to be history matched. It may be possible to lump the capillary pressure effects into the rock pressure correction. Capillary pressure and the rock pressure correction seem to have the same effect on the solution. If capillary pressure is necessary, then a linear function of temperature and water saturation should be adequate to describe its effects. For the Athabasca test runs the capillary pressure is zero.

The Cold lake history match, presented in the next Chapter, is based on the data provided by Denbina, Boberg and Rotter (1987). If a parameter is not mentioned in the following table (Table 4.2), then the same value for the Athabasca bitumen is used (described earlier). The relative permeability curves are provide in Table 4.3.

Table 4.2 History Match Parameters for Cold Lake Production.

Fluid Properties

Gas initial mole fraction in oil	0.8
Water saturation, initial	0.2
Oil saturation, initial	0.8
Gas saturation, initial	0.0
Temperature, initial	20 °C
Initial Pore Pressure	3.6 MPa

Injection

Steam, 73% quality	150 m ³ /day
Pressure	6.4 MPa
Temperature	282 °C
Injection and production	Bottom grid, first column
Injection period	50 days
Production, Back pressure	70 days 400 psia (2.8 MPa)

Mehrotra's Viscosity Parameters (Cold Lake Bitumen)

gas, oil	
b_1	-0.89 9.439
b_2	-0.06 -3.552
mixing rules, A_0 , A_1	-1.34 0.0143

Fracture parameters

A_d	0.6 m ⁻²
Overburden stress	7.8e6 Pa/m ²
Poisson's ratio, initial	0.2
Temperature correction factor	0.0005

Table 4.2 Continued

Capillary Pressure (Pa)

$$P_c = ((30-130*(S_w-.06))*(150.0-T)/150)*6873.0$$

where T is the temperature (°C)

The Capillary pressure is zero if T > 150.0

Grid System

Pay Zone	46 m
Grid, x direction	10, 10, 15, 20, 30, 30
	20, 15, 10, 10 m
Grid, y direction, Bottom to Top	14, 13, 9, 9 m
Grid, z direction	20 m

Table 4.3 Relative Permeability Curves, Cold lake Reservoir

S_w	k_{rw}	k_{row}	1.0-Sg		
			sl	k_{rg}	k_{rog}
0.06	0.000	1.000	0.00	1.00	0.00
0.15	0.008	0.900	0.10	0.90	0.10
0.20	0.014	0.800	0.20	0.50	0.20
0.21	0.016	0.790	0.30	0.40	0.40
0.25	0.048	0.700	0.50	0.30	0.50
0.30	0.068	0.600	0.60	0.25	0.60
0.40	0.091	0.500	0.80	0.10	0.70
0.50	0.120	0.400	0.90	0.09	0.80
0.60	0.140	0.300	0.95	0.005	0.90
0.70	0.165	0.015	0.995	0.00	0.94
0.75	0.179	0.000	1.00	0.00	1.00

Chapter 5

Results and Discussion

5.1 Sensitivity Studies for Fracture Parameters

5.1.1 Effective Heat Transfer Area Coefficient

The value of effective heat transfer area coefficient, " A_d ", has a strong influence on the dispersion in the reservoir. The lower the area, the higher the dispersion in the reservoir. The temperature of the production can be matched easily with this parameter. Figure 10 shows the values of the temperature production with different values of " A_d ". The higher the value of " A_d ", the higher the production temperature. More energy is absorbed from the fracture, and the flow has more Darcy flow characteristics with higher values of " A_d ".

The slope of the production temperature curve is very interesting (after a 50 day injection into the same well)(Figure 10). When the heat transfer area is low, dispersion is high in the reservoir, the production temperature increases with time. This is due to water enthalpy and convection cells in the grid blocks near the well bore. With high dispersion, the matrix pressure gradient is so low that matrix water can flow counter current to the steam flowing in the fractures. These gravity driven convection cells result in higher temperatures at the top of the formation even though injection is at the bottom. However, higher values of " A_d " increase the pressure drop in the matrix, stopping this flow. As the dispersion decreases, the production temperature profile has an increasingly

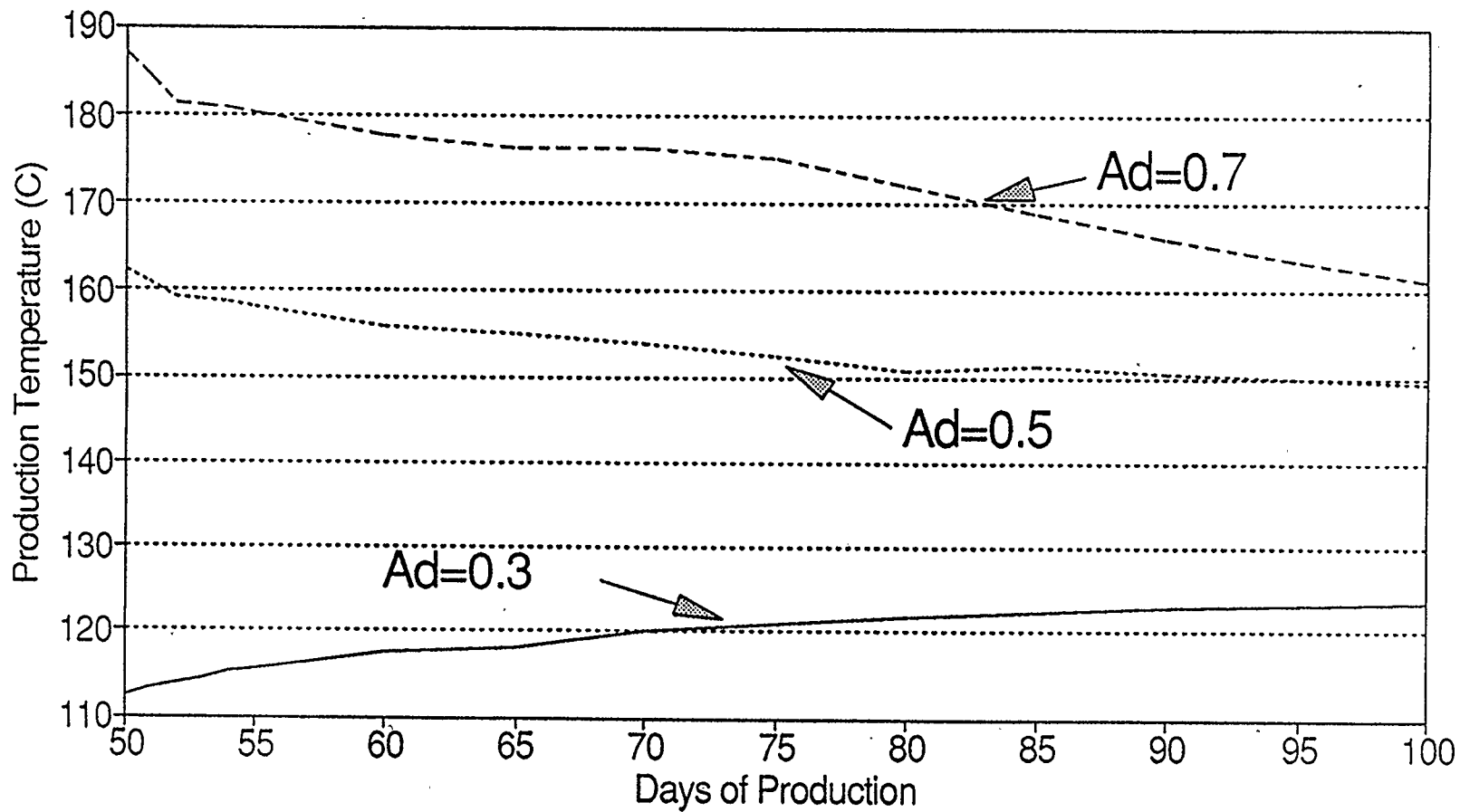


Figure 10 Effects of Dispersion Coefficient
On the Temperature of the Produced Fluids

negative slope. This slope provides some information on the permeability and the capillary pressure of the water near the well bore. Also, some information on the path of the fracture (i.e. gravity override) in the reservoir can be determined by matching the slope of the production temperature curve.

The higher the dispersion in the reservoir, the lower the production temperature. It is not desirable to have the production temperature low since the higher oil viscosity reduces the amount of oil produced. On the other hand, too little dispersion results in smaller volumes of the reservoir being heated. The injection rate can be optimized to maximize the oil steam ratio. As it will be shown later, the rate of injection has an effect on the dispersion in the reservoir. Oil production with various dispersion factors is given in Table 5.1. These values are the model predicted cumulative production after a period of 50 days. The largest value of 75.8 m³ represents less than 6% recovery.

Table 5.1 Predicted Effect of Dispersion on Production of Bitumen

Heat Transfer Area Coefficient " A_d "	Cumulative Production (m ³)
$A_d = 0.3$	6.09
$A_d = 0.5$	36.26
$A_d = 0.7$	75.80

The dispersion in the reservoir strongly affects the temperature near the producer. Less dispersion (higher values of " A_d ") results in higher temperatures near the well bore. Higher temperatures translate into lower viscosity of the oil.

Therefore, more of the bitumen or oil near the well bore is produced.

The parameter, " A_d ", is determined from the temperature of the grid block near the well bore. The heat transfer area deeper in the reservoir can be determined by relating the value of " A_d ", by shape factors (the shape factors depend upon the grid system used). Vertical fractures are assumed to propagate radially from the injector. For the two dimensional cartesian grid system, with equally space grid in the x direction, the shape factor is only a function of the relative heights of the grid blocks. In this way the heat and mass transferred to the grid blocks deeper in the reservoir are estimated.

The heat transferred to the grid block from the fracture is assumed to be limited by conduction. Thermal conductivity of the matrix is not a strong function of fluid and rock properties. Therefore, as long as the energy transferred is conduction limited, the value of, " A_d ", is not sensitive to heterogeneities in the matrix.

Although the model is based on conduction limited heat transfer, some compensation for energy and mass transferred in other ways can be achieved by adjusting, " A_d ". As long as these mechanisms are related to the temperature difference between the fracture and the matrix, the model can account for them. Furthermore, to a degree, the heat transferred is self correcting. If too much heat is transferred, the temperature of the grid block rises reducing the temperature difference, thus reducing the energy flow.

5.1.2 The Temperature Correction Factor Sensitivity

In the fracture pressure equation, there are two adjustable parameters. The first is the initial Poisson's ratio. This can be matched to the initial fracture pressure observed on injection. The temperature dependent variable, v_T , can be matched to the variation in the injection pressure and production results. The impact of the temperature dependent parameter (or the sensitivity) on the solution is shown in the following tables. These tables are for the matrix temperature ($^{\circ}\text{C}$) after 50 days of injection. The numbers across the top of each table are the grid numbers in the horizontal direction. The injection of the steam is at the bottom grid block on the first column.

Table 5.2 Temperature Correction Parameter, $v_T = 0.0001$, Case 1

1	2	3	4	5	6	7	8	9	10
195.	141.	121.	112.	85.3	21.0	11.5	11	11	11
167.	108.	54.4	44.1	29.3	12.8	11.5	11	11	11
162.	108.	28.7	17.1	13.7	11.4	11.2	11	11	11
162.	110.	24.9	13.1	11.6	11.3	11.2	11	11	11

Table 5.3 Temperature Correction Factor, $v_T = 0.002$, Case 2

1	2	3	4	5	6	7	8	9	10
161	145	111	86	46	12	11	11	11	11
162	139	50	29	16	11	11	11	11	11
162.	147	33	15	12	11	11	11	11	11
162.	148	31	13	11	11	11	11	11	11

The high value of temperature in the top block of the first column, is a result of

roll cells. However, it is debatable whether or not this temperature is realistic. However, with a larger temperature correction this artifact is gone, since the temperature correction does not allow the flow of large amounts of steam into the high temperature grid blocks. The larger the value of v_T , the lower the degree of gravity override of the formation. The tongue of heated grid blocks across the top of the reservoir is smaller in case 2. The temperature in the heated zone around the injector is higher.

In case 2, it is expected that the higher temperatures in the second column would translate to better production of the bitumen. Better production is not observed. The bitumen viscosity is not reduced to a low enough level to be drawn to the producer. The majority of the bitumen produced seems to come from gravity drainage of the first column.

5.2 Fracture Growth

The growth of the fracture with time is shown in Figure 11. The graph shows the grid blocks which are fully fractured. In other words, grid blocks which have fracture flow out of them into downstream blocks. There is a fringe of grid blocks around the fractured zone which receive fracture steam but do not give it to others. Initially only an area around the well bore is fractured. However, as the grid blocks near the injector are heated, the fracture zone increases in size. As time goes by, the growth of the fractured zone is primarily across the top of the reservoir.

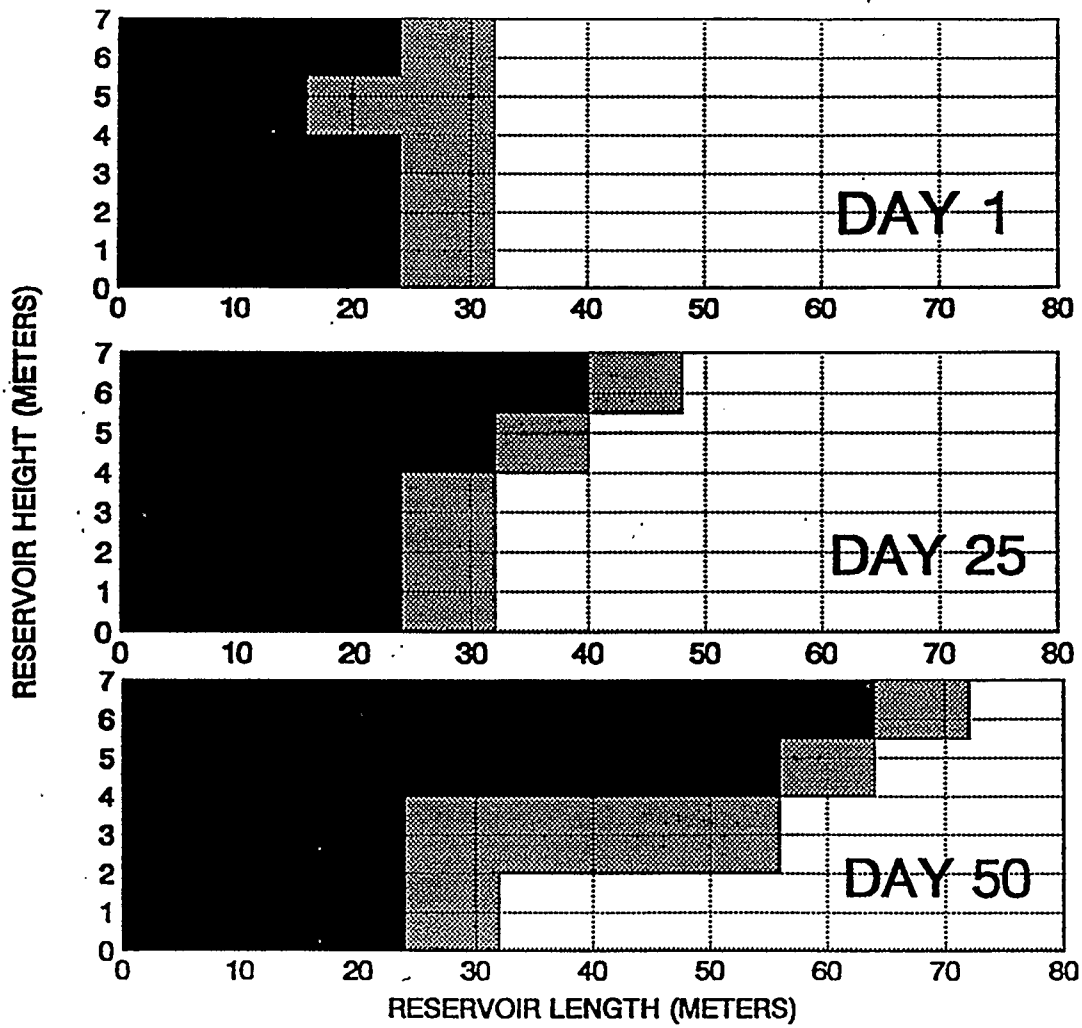


FIGURE 11 FRACTURE GROWTH

As expected, the two dimensional reservoir fractured zone grows with time. However, some qualification of this growth is required for the situation involving three dimensions. The depth of the penetration of the fracture may not be increasing with time. In fact, just the opposite may be true. Usually the initial fractures form in a given direction due to lower stresses. The fracture's path is stabilized by the ease of the propagation of the fracture tip in that direction. Therefore, the fracture will likely grow much further in that direction, before it changes course due to increases in the resistances. However, in a time averaged sense this will not make any difference to the solution. Whether or not the grid block is heated at the end or the beginning of the injection period should make little difference to the temperature distribution in the reservoir. Of course, if a heated region is revisited by the fractures, the fractured zone will grow beyond the previous point of advance.

The high temperature steam advances deep into the reservoir. The matrix temperature lags far behind the advancement of the steam. Table 5.4 shows the estimated fracture temperature ($^{\circ}\text{C}$), in the grid block at 50 days.

Table 5.4 Fracture Temperature

1	2	3	4	5	6	7	8	9	10
256	256	256	255	255	255	254	0.0	0.0	0.0
256	256	253	254	254	255	255	0.0	0.0	0.0
256	256	254	254	253	0.0	0.0	0.0	0.0	0.0
256	256	250	252	0.0	0.0	0.0	0.0	0.0	0.0

The zeros in Table 5.4 indicate that there is no fracture in the grid block. The steam temperature can be compared to the corresponding matrix temperature in Table 5.3.

5.3 The Effect of Injection Rate on the Temperature Distribution

Figure 12 shows the effect of injection rate on the answer. The injection rate is doubled (22 m³ cold water equivalent) for half the time, and compared to the normal injection rate (11 m³ cold water equivalent). Both cases have the cumulative injection (550 m³). Reducing the temperature correction, v_T , to a nominal value makes effects more dramatic. Therefore, this is done here.

The higher rates disperse the thermal energy into the reservoir. At the high rate the dispersion is so high that breakthrough is achieved at the production well. However, the higher rate provides much deeper penetration of the heat into the reservoir. These results are expected.

5.4 The Effect of a Gas Phase on the Production

Figure 13 shows the oil and water production with a gas phase present. Figure 14 shows the production when a gas phase is not present. The production with a gas phase has a lower production rate initially. The lower rate is due to the gas flowing out of the well, decreasing the relative permeability to the bitumen. However, the lower initial rate is compensated

TWO DIMENSIONAL RESERVOIR TEMPERATURE ($^{\circ}\text{C}$)
PROFILE WITH DIFFERENT INJECTION RATES FOR
THE SAME TOTAL INJECTION (550 M^3)

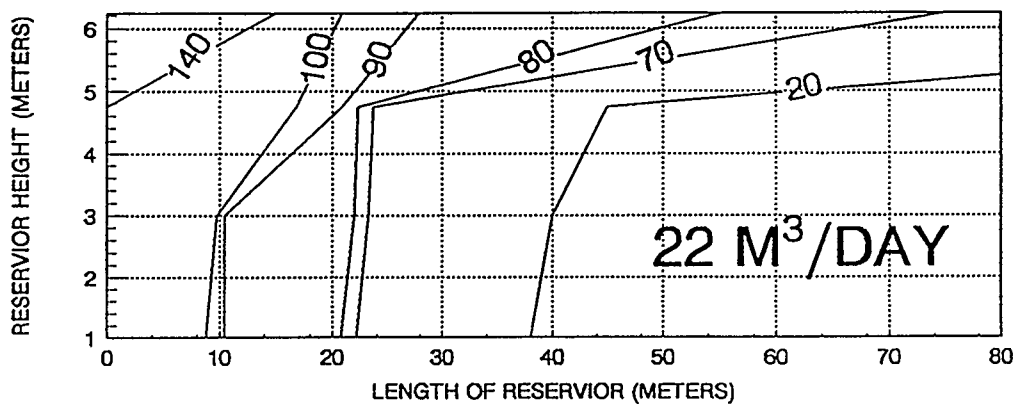
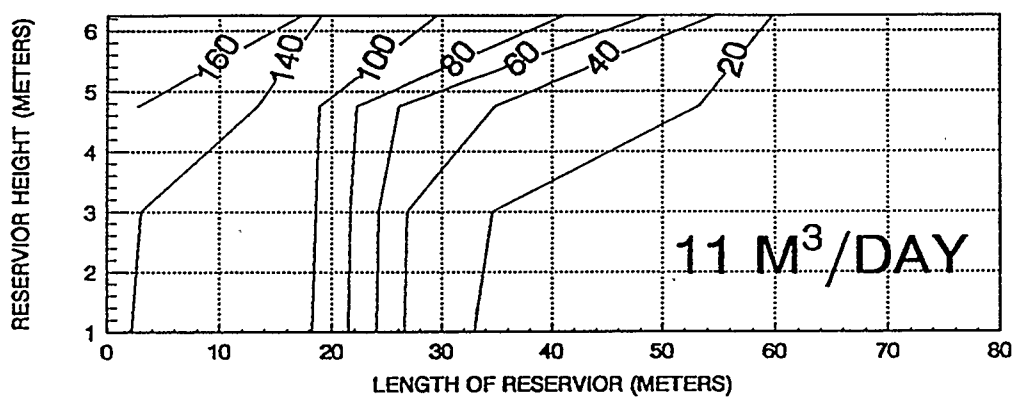


FIGURE 12 EFFECT OF INJECTION RATE ON
RESERVOIR MATRIX TEMPERATURE

PRODUCTION RATE AFTER 1st CYCLE OF STEAM INJECTION
INITIALLY GAS SATURATED RESERVOIR

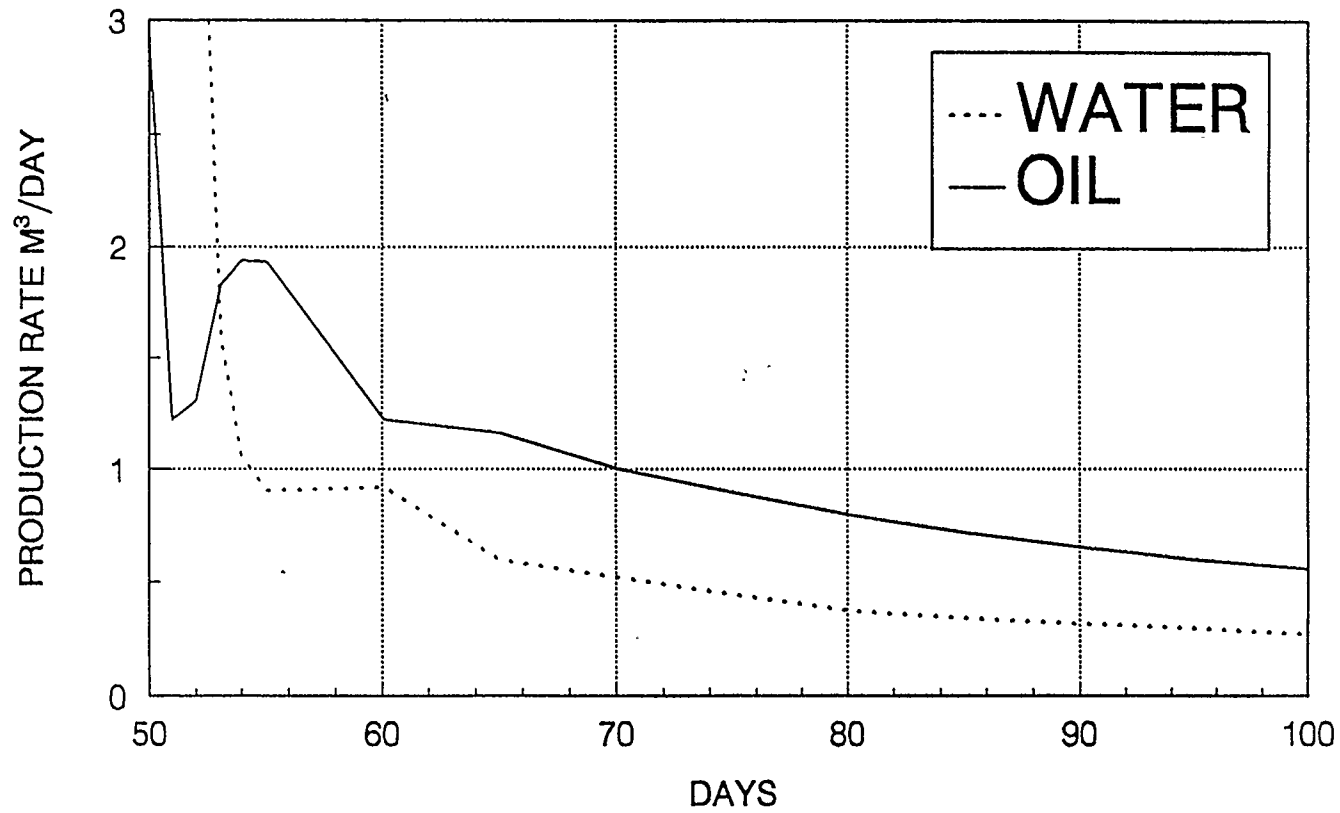


FIGURE 13 GAS SATURATED PRODUCTION

PRODUCTION RATE AFTER 1st CYCLE OF STEAM INJECTION
INITIALLY UNSATURATED RESERVOIR

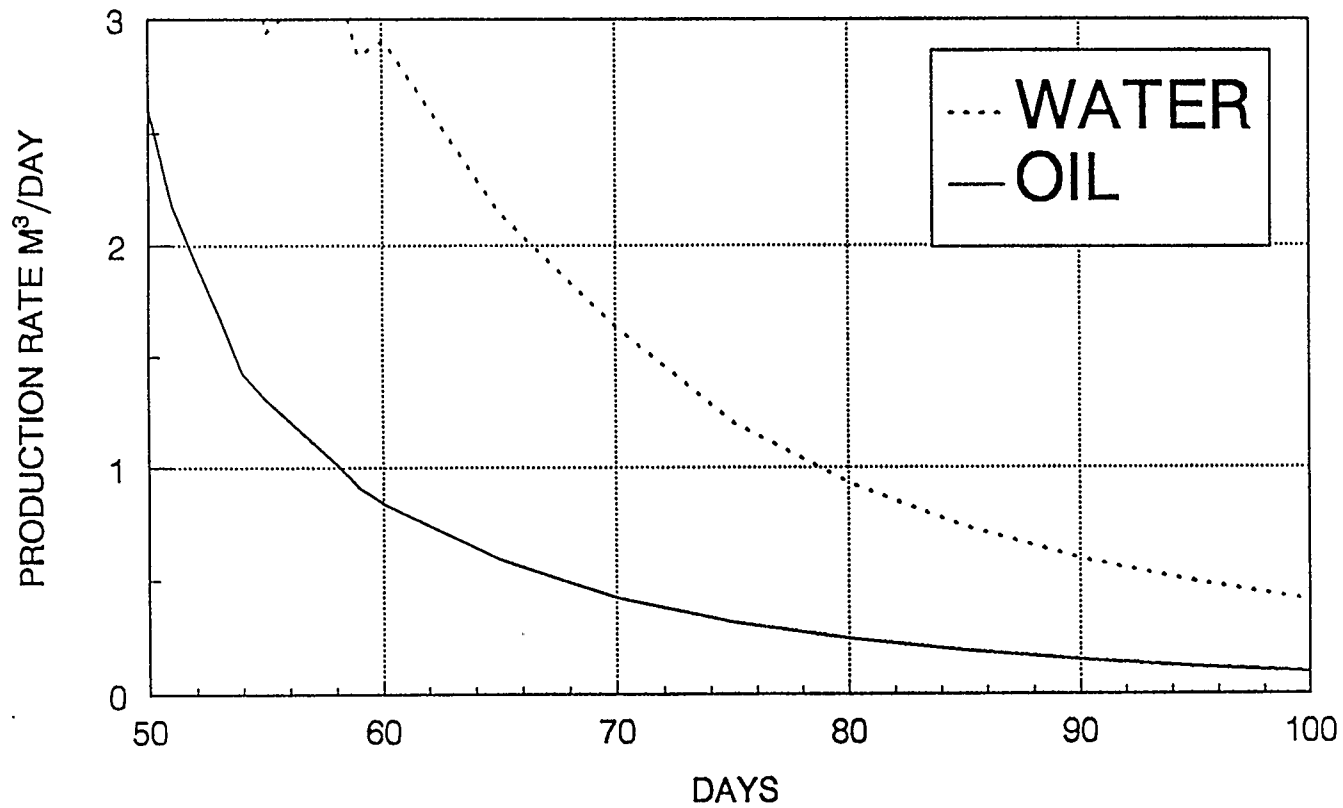


FIGURE 14 UNSATURATED RESERVOIR PRODUCTION

later by the maintenance to the production pressure. More oil is produced in the long run with the gas phase present. Furthermore the water production is also reduced which improves the overall efficiency of the process. This is due to water being pushed away from the well bore by the formation of the gas during injection.

When there is no gas phase, most of the energy for production comes from the compressibility of the reservoir. If the degree of disruption around the well bore is high, along with large hysteresis in the porosity, then the production rate falls off rapidly. In actuality a reservoir with no gas phase after steam injection is probably rare.

5.5 The Effect of Grid Size on the Production Curves

Figure 15 shows the production rate from a grid system with only two grid blocks in the vertical direction. Figure 14 shows the production with four grid blocks in the vertical direction. The top two grid blocks of the four grid block system are lumped into one, along with the bottom two. Comparisons of Figures 14 and 15 show that the production profiles are very similar. This is achieved without any adjustment to any other parameters. The main reason why the production is the same is that the temperature in the first column of grid blocks is nearly uniform. Thus, fewer grid blocks are necessary to simulate the production profiles. This means the simulation can be done much faster.

The case shown is an idealized best case scenario. As mentioned

PRODUCTION RATE AFTER 1st CYCLE OF STEAM INJECTION
INITIALLY UNSATURATED RESERVOIR
TWO GRID BLOCKS IN VERTICAL DIRECTION

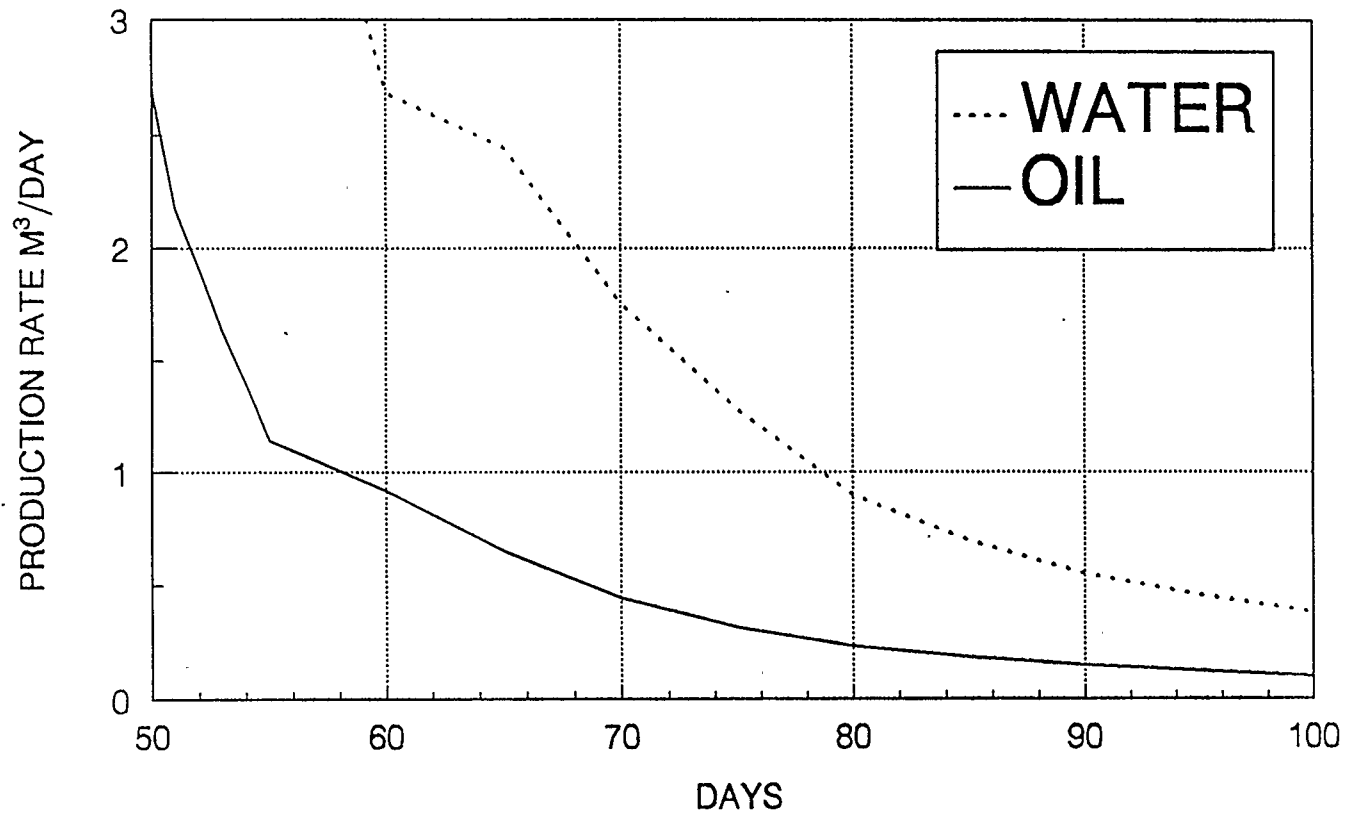


FIGURE 15 UNSATURATED RESERVOIR PRODUCTION

before, it is unlikely that a steamed reservoir will have no gas phase. When a gas phase is present, the profiles do not match as well. Some manipulation of the relative permeabilities is necessary to get the production curves to match, as is usually the case when using different grid block sizes. If the dispersion is such that there is a large temperature gradient in the first column, then it is nearly impossible to match the production of four grid blocks with two. In these circumstances, more grid blocks should be considered rather than fewer.

The size of the grid blocks in the horizontal direction has an impact on the answer. Smaller grid blocks lead to more gravity override of the formation by the fractures. Dispersion is enhanced when the grid block is larger in the horizontal direction. This is true for the matrix as well as the fracture. To insure that the results are reasonable, the grid blocks must not be so large that they exceed the fracturing extent. The limiting case in this matter is the bottom grid block nearest the injector.

The production rates are also affected by smaller grid blocks. The size of the grid blocks on production are limited to how adjustable the relative permeability curves are. Generally, if the relative permeabilities can be adjusted to match the production rates, then the grid block size is considered to be within the range of acceptability.

5.6 The Effect of Injection of Ethane and Steam on the Oil Viscosity

The viscosity of the bitumen is affected by the gas dissolved in it. The

following Tables (5.5 and 5.6) show the viscosity of Athabasca bitumen with and without the consideration of the dissolve gas. In the first case Mehrotra's (1990) mixing rule for the viscosity is enabled. In the second case, the viscosity is only a function of temperature. In both cases, 5 percent ethane gas is injected along with the steam. The characteristic gas is set to ethane for the purposes of the K values.

Table 5.5 Case 1, Viscosity (Pa·s) with Dissolved Ethane Considered.

1	2	3	4	5	6	7	8	9	10
0.017	0.031	0.062	0.095	0.297	1.84	85.0	148	148.	153
0.019	0.053	1.29	2.54	14.1	53.5	145	334	247	155
0.019	0.042	8.4	35.47	94.53	507.9	1260	1272	1276	551.6
0.018	0.035	5.4	145.6	1036	1240	1273	1278	1281	1283

Table 5.6 Case 2, Viscosity (Pa·s) without Gas Viscosity Reduction.

1	2	3	4	5	6	7	8	9	10
0.020	0.043	0.11	0.183	.8523	9.633	1511	3225	3170	3310
0.021	0.081	7.1	15.53	134.5	842	3301	3534	3502	3370
0.021	0.057	70.6	577.9	1980	3262	3665	3701	3714	3629
0.020	.046	35.4	1221	2966	3600	3705	3722	3730	3736

The comparison of the viscosity is complicated by the fact that the temperature distribution is slightly different between the two cases. In view of the high sensitivity of the viscosity to temperature, this slight difference will in turn influence the viscosity profile. However, the differences are only a couple of degrees. Another consideration is the pressure in the two systems. The

pressure profile has an effect on the amount of gas dissolved in bitumen.

Again the pressures do not match, but are within 30 psia (210 Kpa). Therefore comparisons can still be made, but some leeway must be given for the values.

At higher temperatures (first column), the gas has little effect on the viscosity. This is mainly because the amount of gas dissolved in the oil is very low at these temperatures. Deeper in the reservoir the effect of the ethane gas on the viscosity is clearly demonstrated. The viscosity can be an order of magnitude less with gas viscosity reduction. Even though the reduction of the viscosity is large, it is no where near the level required to make the oil mobile. A more powerful viscosity reducing gas is required to make Athabasca bitumen mobile deeper in the reservoir.

Although the viscosity of the bitumen is greatly reduced near the well bore by the temperature, it still is very viscous. The oil viscosity is nearly 20 centipoise (mPa·s) near the well bore. This is nearly 100 times more viscous than the water at this temperature. Unless the water and gas saturations are very low, the only fluids produced are gas and water. If water is being supplied to the well from some source, it is unlikely that the production will be very good. Oil production is best if the oil is allowed to drain by gravity to the producer.

5.7 History Match to Cold Lake Data

Denbina, Boberg and Rotter (1987) studied the early cycles of steam stimulation at Cold Lake using numerical simulation. The steam condensate

has a tendency to flow easily into the reservoir, but does not flow back to the well on production. Dietrich (1981) simulates this effect with unusual relative permeability curves (the water and oil saturation mobile end point saturations are near 50 %). Denbina et. al. account for this phenomena by introducing hysteresis into the relative permeability curves. This enables flow of water into the reservoir but not back. It is difficult to envision a mechanism for this hysteresis in the relative permeabilities. In fact, it would appear likely, that the flow back to the well would be less restricted, since the matrix disrupts and expands increasing the permeability and the saturation of water, respectively. In this history match, another possible mechanism is demonstrated. The fracturing model developed in this work along with capillary pressure and the formation of a gas phase are used to match the production profiles.

Figure 16 compares the oil (bitumen) production rate of the model and the reservoir. The match to the data is reasonable. Although, there was some difficulty reading the data off the graph, the trend is correct and the model production rate is always within a few m^3/day of that of the reservoir. Figure 17 compares the cumulative production rates of the water and the oil. Given that there was a lot of difficulty in reading the data from the provided graph, again the trends are correct and the cumulative production curve for both the water and the oil are reasonably close.

This history match was done with fixed relative permeabilities (Table 4.3). The end points of the water permeability curve are is similar to what Farouq Ali

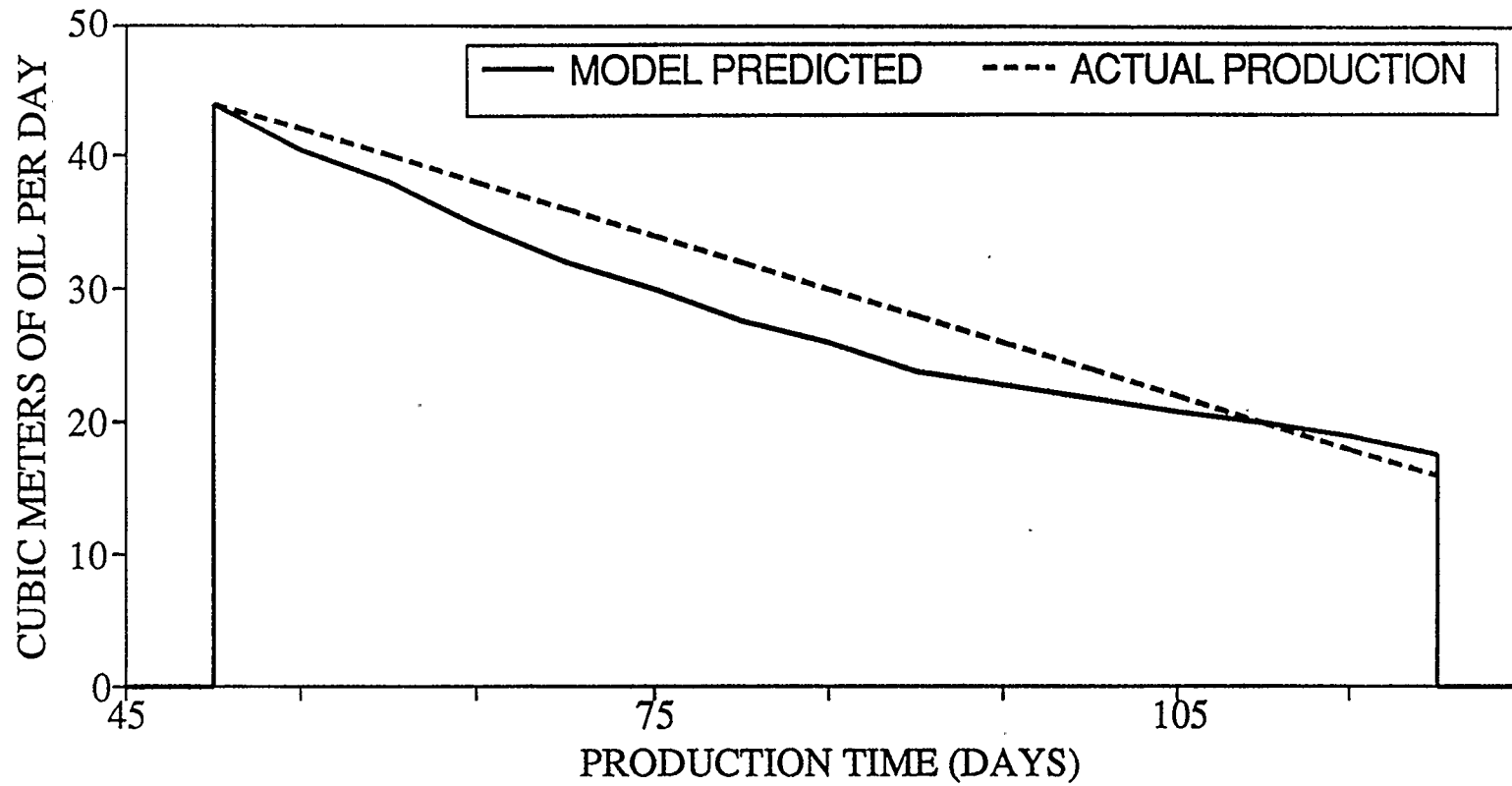


FIGURE 16 FIRST CYCLE HISTORY MATCH
OIL PRODUCTION RATE

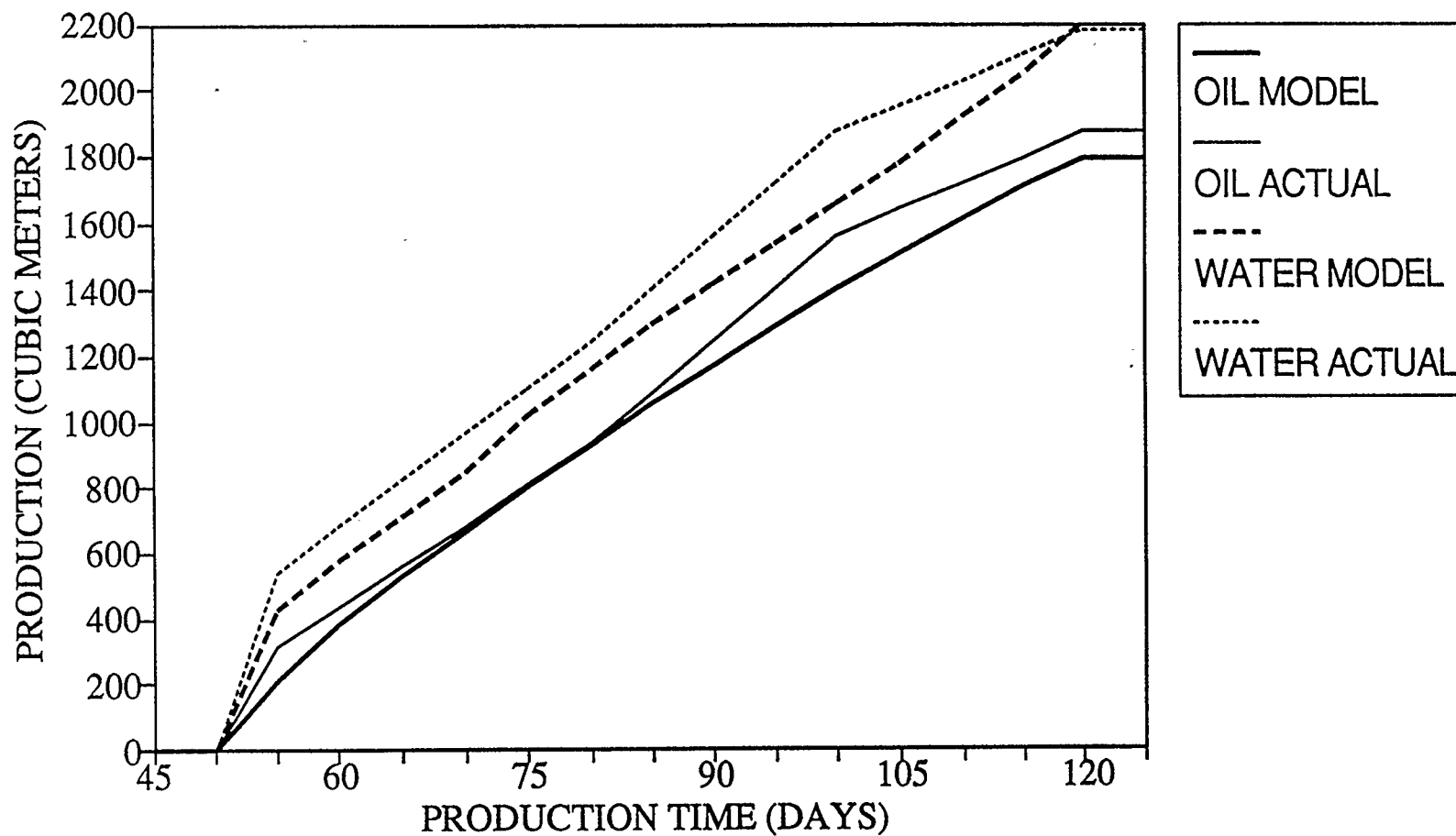


FIGURE 17 FIRST CYCLE HISTORY MATCH
CUMULATIVE OIL AND WATER PRODUCTION

et al. (1985) found in the lab. On injection, the flow into the reservoir is primarily in the fractures. This allows the steam and its condensate to penetrate deep into the reservoir. On production, however, the flow back to the well bore is in the matrix, since the fractures are closed. The fracture flow on injection does not cause a build up of the water saturation in the grid block near the injector. Furthermore, the formation of a gas phase in the grid blocks near the injector, pushes the water out of the grid blocks. The water is further eliminated by the thermal expansion of the oil. The net result is that there is a very low water saturation in the grid blocks near the injector. On production the low water saturation is maintained in the production grid block by the influx of oil from grid blocks above, due to gravity drainage. In addition, the capillary pressure of the water is much lower in the hotter zones (Farouq Ali et al., 1985). Higher capillary pressure of the water deeper in the reservoir will prevent the water from flowing through the hot zone to the well (capillary pressure holds water). In this way the water does not flow to the producer and there is no need for hysteresis in the relative permeability curves or to use unusual relative permeabilities.

Chapter 6

Conclusion and Recommendations

The fracturing of the reservoir produces dispersion. This dispersion lowers the inter-grid gradients and allows the use of larger grid blocks than is possible with Darcy flow. Depending on the magnitude of the dispersion, the size of the grid blocks can be adjusted accordingly. However, grid block size is also dependent on other factors. These other factors (i.e. production pressure and rates, path of fracture flow) may also limit the size of the grid blocks.

The fracturing model developed in this work is an improvement over other fracturing models for unconsolidated sands. The areas where the model does quite well are as follows.

1. The model requires no extra equations to be solved inside the Newton-Raphson set. This keeps the computer time requirement of the program to a minimum. Furthermore, consistency of the solution is improved and hence allowing larger time steps.
2. The degree of dispersion of the reservoir under a given injection rate can be history matched easily. This provides a measure of how deep the reservoir is being penetrated by the steam.
3. The gravity override of the fractures over the top of the formation can be realistically modelled. Although the physics of the model is nowhere near exact, it is felt that the model is a reasonable estimate of the process.

The main problem with the model is the difficulty in history matching the degree of gravity override. Other variables within the thermal simulator are also difficult to history match. These history matching problems are due to the small amount of information obtained from the reservoir. The complexity of the thermal model means that there are many more parameters to be fitted than available information. The addition of the temperature dependent variable makes the history match that much more difficult. However, there is some convoluted information to which the parameter can be fitted (i.e. slope of the production temperature curve, injection pressure, production profile). If the other parameters can be determined from other sources (e.g. lab, experience, etc) then the gravity override can be history matched.

The inclusion of a condensible gas component appears to have a very strong effect on the solution. For example, the impact of the gas component on the bitumen viscosity is demonstrated. If the gas component's effects are ignored it is difficult to get good results from the simulator. The exception to this is the case where the bitumen is completely dead.

References

Allen T. and Roberts A., Production Operations, Oil and Gas Consultants International, 1982, Vol. 2, Chapter 8, 2nd Edition.

Aziz K. and Settari A., Petroleum Reservoir Simulation, Applied Science Publishers Ltd., 1979.

Belgrave J.D.M., Moore R.G., Ursenbach M.G. and Bennion D.W., "A Comprehensive Approach to In-Situ Combustion Modelling", 7th Symposium on Enhanced Oil Recovery, Society of Petroleum Engineers, Tulsa, Oklahoma, April 1990, 751-762.

Bennion D.W., Moore R.G. and Thomas F.B., "Effect of Relative Permeability on the Numerical Simulation of the Steam Stimulation Process", The Journal of Canadian Petroleum Technology, Vol 24, No. 2, April 1985, 40-45.

Brantferger K.M., Pope G.A. and Sepehrnoori K., "Development of a Thermodynamically Consistent, Fully Implicit, Equation-of-State, Compositional Steamflood Simulator", Proceedings of the SPE Symposium on Reservoir Simulation, Anaheim, CA, Society of Petroleum Engineers, February 1991, 471-479.

Burden, R.L., Faires, J.D. and Reynolds, A.C., Numerical Analysis, Prindle, Weber and Schmidt, Boston, Second Edition, 1981

Butler R., "The expansion of tar sands during thermal recovery", The Canadian Journal of Petroleum Technology, Vol 25, No. 5, October 1986, 51-56.

Butler R., Thermal Recovery of Oil and Bitumen, Prentice Hall, New Jersey, 1991

Coats, K.H., "In-Situ Combustion Model", Society of Petroleum Engineers Journal, Vol 20, No. 3, December 1980, 533-554.

Denbina, E.S., Boberg, T.C. and Rotter, M.B., "Evaluation of Key Reservoir Drive Mechanisms in the Early Cycles of Steam Stimulation at Cold Lake", SPE 16737, Dallas (1987), Society of Petroleum Engineers.

Dietrich, J.K., "Relative Permeability During Cyclic Steam Stimulation of Heavy-OIL Reservoirs", Journal of Petroleum Technology, October 1981, 1987-1989

Forsyth Jr., P., Rubin, B. and Vinsome, P.K.W., "The elimination of the constraint equation and the modelling of the problems with a non-condensable gas in steam simulation", The Journal of Canadian Petroleum Technology, Vol

20, No. 4, December 1981, 63-70.

Farouq Ali S.M and Polikar M., Ferracuti F., Decastro V., and Puttagunta. R., "Effect of Temperature on the Bitumen-Water end point Relative Permeabilities and Saturations", The Journal of Canadian Petroleum Technology, Vol 25, No. 5, October 1986, 44-50.

Ito, Y., "The Introduction of the Microchanneling Phenomenon to Cyclic Steam Stimulation and Its Application to the Numerical Simulator", Society of Petroleum Engineers Journal, Vol 24, No. 4, August 1984, 417-430.

Mehrotra A.K., Mallika S. and Svrcek W., "Bitumen Density and Gas Solubility Prediction Using the Peng-Robinson Equation of State", AOSTRA Journal of Research, Vol. 1, Number 4, 1985, 215-229.

Mehrotra A.K., and Svrcek W.Y., "Viscosity, Density and Gas Solubility Data for Oil Sand Bitumens. Part 1: Athabasca Bitumen Saturated with CO and C₂H₆", AOSTRA Journal of Research, Vol. 1, Number 4, 1985, 264-268.

Mehrotra A.K., "Mixing Rules for the Predicting the Viscosity of Bitumen Saturated with Pure Gases", The Canadian Journal of Chemical Engineering, Vol 20, February, 1992, 165-171.

Pethrick W.D., Sennhauser E.S. and Harding T.G., "Numerical Modelling of Cyclic Steam Stimulation in Cold Lake Oil Sands", The Journal of Canadian Petroleum Technology, Vol 27, No.6, December 1988, 89-95.

Green D. and Perry, R., ed., Perry's Chemical Engineering Handbook, McGraw-Hill Book Company, New York, 6th edition, 1984.

Redford D.A., "In-situ recovery from the Athabasca oil sands - past experience and future potential", The Journal of Canadian Petroleum Technology, Vol 24, No. 3, June 1985, 52-62.

Reid R.C., Prausnitz J.M. and Sherwood T.K., The Properties of Liquids and Gases, McGraw-Hill Book Company, 1977, Third Edition.

Rubin, B. and W. Buchanan, "A General Purpose Thermal Model", Society of Petroleum Engineers Journal, April 1985, 202-214.

Settari, A. and Raisbeck, J.M., "Analysis and Numerical Modelling of Hydraulic Fracturing During Cyclic Steam Stimulation in Oil Sands", Journal of Petroleum Technology, November 1981, 2201-2212.

Schmidt, E., ed., Properties of Water and Steam in SI-Units, Springer-Verlag
New York Inc., 1969.

Thomas, G.W, "An Extension to the Pseudo Function Concept", 1983, Society
of Petroleum Engineers, SPE 12274

Xu Y. and Hepler L., "Henry's Law Constants and Thermodynamic Properties of
Gases and Vapours in Bitumens", The Canadian Journal of Chemical
Engineers, Vol. 68, December 1990, 1024-1031.

Appendix A

Conservation Equation for the Matrix

The flow of fluid in porous media is described by Darcy's equation. The molar flux (molar flow per unit area per unit time), m , is given by

$$m = \frac{K}{\mu} \rho \frac{dP}{dL} \quad \text{A1}$$

where K is the permeability of the porous media, μ is the viscosity of the fluid, ρ is the molar density of the fluid, A is the cross sectional area, P is pressure and L is the length. An extension to Darcy's equation to account for multi-phase flow of component i is provided by the following:

$$m_i = \sum_{j=1}^3 \frac{K k_j}{\mu_j} \rho_j x_{ij} \frac{dP}{dL} \quad \text{A1}$$

where k_j is the relative permeability (fraction of the total permeability that the phase sees) of phase j and x_{ij} is the mole fraction of component i in phase j . Usually there are three "mobile" phases: water, oil and gas. The summation of the flow of component i in all phases gives the total flow.

A mole balance of component i about a finite element is represented below (Figure A1).

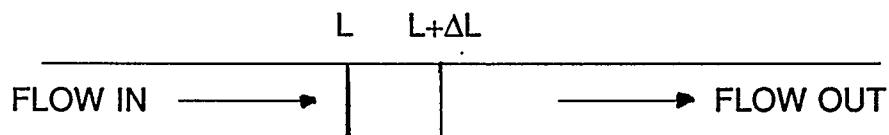


Figure A1

With injection or production terms, q_i (moles per volume per unit time), and reactions, the mole balance on component i at any instant in time, t , yields the following equation:

$$(m_i|_L - m_i|_{L+\Delta L})A\Delta t + q_i\Delta V\Delta t + r_i\Delta t\Delta V = \frac{\partial n_i}{\partial t}\Delta t \quad \text{A3}$$

where n_i is the number of moles of component i in the finite volume, ΔV , at time t and r_i is the rate of formation of component i per volume. In porous media the number moles of component i per volume, n_i , is given by

$$n_i = \phi \sum_{j=1}^{N_p} S_j x_{ij} \rho_j \quad \text{A4}$$

where ϕ is the porosity of the control volume (void fraction of the rock) and S_j is the saturation of the fluid phase j (volume fraction of the pore volume).

Substituting for n_i and m_i and dividing through by $\Delta V\Delta t$ and taking limit as ΔL goes to zero, Equation A3 becomes

$$\frac{\partial \left(\sum_{j=1}^3 \frac{Kk_j}{\bar{\mu}_j} \rho_j x_{ij} \left(\frac{\partial P}{\partial L} + \rho_j g \Delta z + \frac{\partial P_{cj}}{\partial L} \right) \right)}{\partial L} + q_i + r_i = \frac{\partial \left(\phi \sum_{j=1}^{N_p} \rho_j S_j x_{ij} \right)}{\partial t} \quad \text{A5}$$

where P_{cj} is the capillary pressure and $\rho_j g \Delta z$ is the gravity effect on phase j .

Conversion to finite difference equation requires the use of approximate derivatives. Both sides of the equation are multiplied by ΔV . The transmissibility factor, τ , is used to replace KA/L . The resulting equation is

$$\frac{\Delta V}{\Delta t} \delta \left[\phi \sum_{j=1}^{N_p} \rho_j S_j x_{ij} \right] = \sum_{j=1}^{N_p} \Delta \tau_{pj} \rho_j x_{ij} \frac{k_{ri}}{\mu_j} (\Delta P_m + \Delta P_c - \gamma_j \Delta z) + \sum_{n=1}^{N_{rea}} q_{in} - q_{ip} \quad A6$$

where q_{in} is the rate of formation or disappears component i in each of the N_{rea} reactions.

Apparent in Equation A6 are three factors which result in changes in the number of moles in the control volume. These are the convection flow from other grid blocks (Darcy flow), the injection of fluids and the reactions. Another major factor is the thermodynamics of the fluids. The phase distribution coefficients, K values, are calculated from correlations. Through the K values, the mole fraction in a phase is related to the mole fraction in another phase. The hydrodynamic, reactions and the thermodynamic equilibrium portions of the equation must all be satisfied simultaneously.

The matrix energy balance equation can be found in a similar fashion.

Appendix B

Maltenes Sliding Scale

The initial normalized maltenes mole fraction in the oil phase is the basis for the scale. The mole fraction is normalized by

$$X_{mn} = \frac{X_m}{1.0 - \sum X_{go}} \quad \text{B1}$$

where X_m is the maltenes mole fraction and X_{go} is the mole fraction of the gas component in the oil. The fractional deviation, F_c , from the initial normalized mole fraction, X_{mni} , is given by

$$F_c = \frac{X_{mn}}{X_{mni}} \quad \text{B2}$$

Any deviation from one is assumed to occur in the lightest mole fraction in the maltenes cut. The lightest component's mole fraction, y_L , is given by

$$y_L = F_c - \sum_{i=1}^{n-1} y_i \quad \text{B3}$$

where $n-1$ is the number of components heavier than the lightest.

The maltenes cut is assumed to be subdivided into four pseudo components. The molecular weights, critical properties and mole fractions of each component are given by Mehrotra, Sarkar, and Svrcek(1984).

Component	Mole Fraction	NBP K	Pc MPa	Tc K
Lightest	.0682	453	2.46	637
2nd	.1400	523	1.95	704
3rd	.0335	653	1.54	801
Heaviest	.7583	773	1.43	972

By applying Riedel's vapour pressure (Sherwood et al. 1977), K values for each for the pseudo components are found. The effective K value, K_e , for the mixture is then found from

$$K_e = \frac{\sum_{i=1}^n K_i y_i}{\sum_{i=1}^n y_i}$$

B4

Appendix C

Condensable Gas Sliding Scale

The initial mole fraction of the gas in the oil phase is the bases for the scale. It is assumed that the characteristic gas carbon number is relative to how much gas is dissolved in the oil. The lower the fraction of gas in the oil, the lower the volatility of the gas. In order to find a characteristic K value of the gas, it is necessary to know the distribution of the various gases in solution. This information should not be too difficult to obtain from the field. In this case, a distribution of carbon number, CN , of gas is conceived to have the form

$$CN = CNI - 1.0 + e^{(efac(1.0 - xfac))} \quad C1$$

where CNI is the initial carbon number, $efac$ is the exponential factor and $xfac$ is the fraction of the initial gas mole fraction in the oil phase. The exponential factor controls the rate at which the carbon number increases with decreasing dissolved gas.

The data for the Henry's constants, K_H , is provided by Xu and Helper. The data is fitted to the equation form

$$\ln K_H = \left(\frac{A1(CN)}{T} \right) + B1(CN) \quad C2$$

where T is the temperature in Kelvin. The functions of carbon number ($A1$ and $B1$) are linear and give a good fit to the data, except for methane. The error in methane however is not serious. These linear functions are as follows

$$A1(CN) = 528.04452 CN + 181.93210$$

C3

$$B1(CN) = 0.60956 CN + 11.14025$$

C4

The K values are calculated as the ratio of the Henry's constant to the pressure of the system. In the program, the K values are linearized about the previous time step state variables. This improves the numerical performance of the simulator.

Appendix D

Computer Time

The required computer time depends on the problem. For the Cold Lake history match the time requirements vary depending on whether or not a gas phase is present. Without the a gas phase, the 50 day injection period and the 70 day production period require about 5 minutes of CPU time on an IBM 6000 work-station. The average time step was 0.5 days. When a gas phase is present, the computer time requirements increase to about 20 minutes, with an average time step of 0.12 days.

The overall improvement in the speed of the simulator achieved in this work is very significant. Relative to the performance of the original simulator (with Ito's fracturing model), the modifications in this work has increased the speed 200,000 fold. This is not an indication of how well the present simulator runs, but rather how poorly the original simulator ran. It is difficult to say how much of the increase in the speed is due to which modification. However, it can be estimated that at least a 10 fold increase was achieved through optimizing the code for speed (i.e. reducing array size, etc). A further 10 fold increase was achieved, by using more efficient algorithms (i.e. equation solver). The biggest increase, however, comes from the increase in the time step. The next time step solution guess , consistency, the fracturing model and the formulation all contribute to the increase in the time step.

Appendix E

Water Correlation

The correlation (Schmidt, 1969) can accurately represent the thermodynamic properties of pure water. Its original purpose was to enable the production of extensive steam tables. This accuracy provides consistency to the overall solution of the steam simulator

```
c---- SUBROUTINE WATER
C---- ARGUMENTS
C   INPUT --> P IN Pa, T IN C
C   OUTPUT -> HL ENTHALPY OF LIQUID, VL VOLUME OF LIQUID
C           VP VAPOUR PRESSURE, HG ENTHALPY OF VAPOUR
C           VG VOLUME/KMOLE, PHASE AT INPUTTED P AND T
```

```
SUBROUTINE WATER(P,T,HL,VL,VP,HG,VG,FTYPE)
REAL*8 P,T,HL,HG,S,VL,VG,VP
integer FTYPE
```

```
REAL*8 A(23),SA(12),B0(6),B1(2),B2(3)
REAL*8 B3(2),B4(2),B5(3),B6(2),B7(2),B8(2),B9(7),SB
REAL*8 SB61,SB71,SB81,SB82
REAL*8 K(9),L
REAL*8 PT1,TC1,PC1,VC1,R1,I1
REAL*8 SUM1,SUM2,SUM3,SUM4
REAL*8 SI,E,X,Y,Z,T12,T11,T2,T3,P1,P2,PA
LOGICAL ZONE(6)
```

```
DATA A / 6.824687741E3 , -5.422063673E2 , -2.096666205E4 ,
1      3.941286787E4 , -6.733277739E4 , 9.902381028E4 ,
2      -1.093911774E5 , 8.590841667E4 , -4.511168742E4 ,
3      1.418138926E4 , -2.017271113E3 , 7.982692717 ,
4      -2.616571843E-2, 1.52241179E-3, 2.284279054E-2,
5      2.421647003E2 , 1.269716088E-10, 2.074838328E-7,
6      2.174020350E-8, 1.105710498E-9, 1.293441934E1 ,
7      1.308119072E-5, 6.047626338E-14 /
DATA SA / 8.438375405E-1, 5.362162162E-4, 1.720 ,
```

```

1      7.342278489E-2, 4.975858870E-2, 6.5371543E-1 ,
2      1.150E-6 , 1.5108E-5 , 1.4188E-1 ,
3      7.002753165 , 2.995284926E-4, 2.040E-1 /
DATA B0 / 1.683599274E1 , 2.856067796E1, -5.438923329E1,
1      4.330662834E-1, -6.547711697E-1, 8.565182058E-2/
DATA B1 / 6.670375918E-2, 1.388983801 /
DATA B2 / 8.390104328E-2, 2.614670893E-2, -3.373439453E-2/
DATA B3 / 4.520918904E-1, 1.069036614E-1/
DATA B4 / -5.975336707E-1, -8.847535804E-2/
DATA B5 / 5.958051609E-1, -5.159303373E-1, 2.075021122E-1/
DATA B6 / 1.190610271E-1, -9.867174132E-2/
DATA B7 / 1.683998803E-1, -5.809438001E-2/
DATA B8 / 6.552390126E-3, 5.710218649E-4/
DATA B9 / 1.936587558E2 , -1.388522425E3, 4.126607219E3,
1      -6.508211677E3, 5.745984054E3, -2.693088365E3,
2      5.2357186232E2/
DATA SB,SB61/ 7.6333333E-1, 4.006073948E-1/
DATA
SB71,SB81,SB82/ 8.636081627E-2, -8.532322921E-1, 3.460208861E-1/
DATA K / -7.691234564, -2.608023696E1, -1.681706546E2,
1      6.423285504E1, -1.189646225E2, 4.167117320,
2      2.097506760E1, 1E9, 6/
DATA L / 7.160997524 /
DATA PT1,TC1,PC1,VC1,R1/ 611.2, 647.3, 22120000, 0.00317, 461.51/
DATA TT/ 273.15 /
DATA TRT,TR1,TR2,TR3 / 4.219990731E-1, 9.626911787E-1, 1.333462073,
1      1.657886606/
DATA PRT,PR1,PR2/ 2.763311032E-5, 7.475191707E-1, 4.520795660/

T=T+273.15
I1=R1*TC1/PC1/VC1
PR=P/PC1
TR=T/TC1

BL=((TR2-TR)*PR1+(TR-TR1)*PR2-L*(TR2-TR)*(TR-TR1))/(TR2-TR1)
BLP=(PR2-PR1-L*(TR2-2*TR+TR1))/(TR2-TR1)

SUM1=0.0
DO 100 I=1,5
  SUM1=SUM1+K(I)*(1-TR)**I
100 CONTINUE

BKT=EXP(SUM1/TR/(1+K(6)*(1-TR)+K(7)*(1-TR)**2)-(1-TR)/
1 (K(8)*(1-TR)**2+K(9)))

```

```

VP=BKT*PC1
P1=P
P2=P
PA=P

```

```

IF(P .GT. PC1) VP=BL*PC1

```

```

ZONE(1)=.FALSE.
ZONE(2)=.FALSE.
ZONE(3)=.FALSE.
ZONE(4)=.FALSE.

```

C--- FINDING ZONE FOR CORRELATION

```

IF (TRT .LE. TR .AND. TR .LE. TR1) THEN
  IF(PR .GE. 0 .AND. PR .LT. BKT) THEN
    FTYPE=2
    ZONE(2)=.TRUE.
    P1=VP
  ENDIF
  IF(PR .GE. BKT ) THEN
    ZONE(1)=.TRUE.
    FTYPE=1
    P2=VP
  ENDIF

ELSEIF(TR1 .LT. TR .AND. TR .LT. 1) THEN
  IF(PR .GT. 1) ZONE(3)=.TRUE.
  IF(PR .GE. 0 .AND. PR .LT. BKT) THEN
    ZONE(2)=.TRUE.
    FTYPE =2
    P1=VP
  ENDIF
  IF(BKT .LE. PR ) THEN
    ZONE(1)=.TRUE.
    FTYPE=1
    P2=VP
  ENDIF

ELSEIF(1.0 .LE. TR .AND. TR .LT. TR2) THEN
  IF (BL .LT. PR .AND. PR .LE. PR2) THEN
    ZONE(1)=.TRUE.
    FTYPE=1
    P2=VP
  ELSE

```

```

ZONE(2)=.TRUE.
FTYPE=2
P1=VP
ENDIF
ELSE
ZONE(2)=.TRUE.
FTYPE=2
P1=VP
ENDIF

```

```

P=P1
p=pa
if(p .gt. vp)p=vp
PR=P/PC1

```

C---- LIQUID CALCULATION

```

Y=1-SA(1)*TR*TR-SA(2)*TR**(-6)
Z=SA(3)*Y*Y-2.*SA(4)*TR+2*SA(5)*PR
IF(Z .LT. 0.0) Z=0.0
Z=Y+Z**.5
SI=A(12)*SA(5)*Z**(-5./17.)+(A(13)+A(14)*TR+A(15)*TR*TR
1  +A(16)*(SA(6)-TR)**10+A(17)*(SA(7)+TR**19)**(-1))-
2  (SA(8)+TR**11)**(-1)*(A(18)+2*A(19)*PR+3*A(20)*PR*PR)-
3  A(21)*TR**18*(SA(9)+TR*TR)*(-3*(SA(10)+PR)**(-4)+
4  SA(11))+3*A(22)*(SA(12)-TR)*PR*PR+4*A(23)*TR**(-20)*PR**3
SUM1=0.0
DO 101 I=2,11
    SUM1=SUM1+(I-3)*A(I)*TR**(I-2)
101 CONTINUE
YP=-2*SA(1)*TR+6*SA(2)*TR**(-7)
E=A(1)*TR-SUM1
E=E+A(12)*(Z*(17*(Z/29-Y/12)+5*TR*YP/12)+SA(4)*TR-
1  (SA(3)-1)*TR*Y*YP)*Z**(-5./17.)+(A(13)-A(15)*TR*TR+A(16)*
2  (9*TR+SA(6))*(SA(6)-TR)**9+A(17)*(20*TR**19+SA(7))*
3  (SA(7)+TR**19)**(-2))*PR-(12*TR**11+SA(8))*(SA(8)+
4  TR**11)**(-2)*(A(18)*PR+A(19)*PR**2+A(20)*PR**3)+A(21)
5  *TR**18*(17*SA(9)+19*TR*TR)*((SA(10)+PR)**(-3)+SA(11)*PR)
E=E+A(22)*SA(12)*PR**3+21*A(23)*TR**(-20)*PR**4
VL=SI*VC1
HL=E*PC1*VC1/1000.

```

C-- VAPOUR CALCULATION

P=P2
 PR=P/PC1
 X=EXP(SB*(1.0-TR))

SUM3=0.0

SUM1=(B1(1)*X**13+B1(2)*X**3)+2.*PR*(B2(1)*X**18+B2(2)*X*X+
 1 B2(3)*X)+3.*PR*PR*(B3(1)*X**18+B3(2)*X**10)+4.*PR**3*
 2 (B4(1)*X**25+B4(2)*X**14)+5.*PR**4*(B5(1)*X**32+
 3 B5(2)*X**28+B5(3)*X**24)

SUM2=4.*PR**(-5)*(B6(1)*X**12+B6(2)*X**11)/(PR**(-4)+
 1 SB61*X**14)**2+5.*PR**(-6)*(B7(1)*X**24+B7(2)*X**18)/
 2 (PR**(-5)+SB71*X**19)**2+6.*PR**(-7)*(B8(1)*X**24
 3 +B8(2)*X**14)/(PR**(-6)+SB81*X**54+SB82*X**27)**2

DO 103 J=1,7

SUM3=SUM3+B9(J)*X**(J-1)

103 CONTINUE

SUM3=11.*(PR/BL)**10*SUM3

SI=I1*TR/PR-SUM1-SUM2+SUM3

SUM1=PR*(B1(1)*(1.+13.*SB*TR)*X**13.+B1(2)*(1.+3.*SB*TR)
 1 *X**3)+PR**2*(B2(1)*(1.+18.*SB*TR)*X**18+B2(2)*(1.+2.*SB*TR)*
 2 X**2.+B2(3)*(1.+SB*TR)*X)+PR**3*(B3(1)*(1.+18.*SB*TR)*X**18+
 3 B3(2)*(1.+10.*SB*TR)*X**10)+PR**4*(B4(1)*(1.+25.
 4 *SB*TR)*X**25+B4(2)*(1.+14.*SB*TR)*X**14)+PR**5*(B5(1)*
 5 (1+32.*SB*TR)*X**32+B5(2)*(1.+28.*SB*TR)*X**28+B5(3)*(
 6 1+24.*SB*TR)*X**24)

T11=1.+12.*SB*TR

T12=1.+11.*SB*TR

T2=SB*TR*14.*SB61*X**14

T3=PR**(-4)+SB61*X**14

SUM2=B6(1)*X**12*(T11-T2/T3)/T3+B6(2)*X**11*(T12-T2/T3)/T3

T11=1.+24.*SB*TR

T12=1.+18.*SB*TR

T2=SB*TR*19.*SB71*X**19

T3=PR**(-5)+SB71*X**19

SUM2=B7(1)*X**24*(T11-T2/T3)/T3+B7(2)*X**18*(T12-T2/T3)/T3+SUM2

T11=1.+24.*SB*TR

T12=1.+14.*SB*TR

T2=SB*TR*(54.*SB81*X**54+27.*SB82*X**27)

T3=PR**(-6)+SB81*X**54.+SB82*X**27.

SUM2=B6(1)*X**12*(T11-T2/T3)/T3+B6(2)*X**11*(T12-T2/T3)/T3+SUM2

SUM3=0.0

DO 105 J=1,7

SUM3=SUM3+(1.+TR*(BLP*10/BL+J*SB)*B9(J)*X**(J-1))

```
105 CONTINUE
    SUM4=B0(1)*TR
    DO 106 J=2,6
        SUM4=SUM4-B0(J)*REAL(J-3)*TR**(J-2)
106 CONTINUE
    E=SUM4+SUM3*PR*(PR/BL)**10-SUM1-SUM2

    P=PA
    T=T-273.15
    VG=SI*VC1
    HG=E*PC1*VC1/1000.
    VP=VP

    RETURN
    END
```